

Efficient K-Means Clustering Algorithm Using Feature Weight and Min-Max Normalization

Ei Ei Phyo

Department of Information Technology
Technological University (Thanlyin),
Myanmar

Ei Ei Myat

Department of Information Technology
Technological University (Thanlyin),
Myanmar

Abstract: Clustering is a process of partitioning a set of data into a set of meaningful sub-classes, called clusters. K-means is an effective clustering technique used to separate similar data into groups based on initial centroids of clusters. In this paper, the proposed algorithm applies normalization prior to clustering on the available data as well as the proposed approach calculates initial centroids based on weights. Experimental results prove the betterment of proposed clustering algorithm over existing K-means clustering algorithm in terms of computational complexity and overall performance.

Keywords: clustering, k-means clustering, min-max normalization, gain ratio, initial centroid

1. INTRODUCTION

Data mining [1] [2] or knowledge discovery is a process of analyzing large amounts of data and extracting useful information. Data mining is widely used in various areas like financial data analysis, retail and telecommunication industry, biological data analysis, fraud detection, spatial data analysis and other scientific applications. Clustering is categorized as one of the data descriptive analysis technique that builds clusters of data objects in such a way that objects in a cluster are closer to each other than the objects of other clusters. K-means uses the concept of Euclidean distance to calculate the centroids of the clusters. This method is less effective when new data sets are added and have no effect on the measured distance between various data objects. The computational complexity of k means algorithm is also very high [1] [3]. K-means is the most popular and best understood traditional clustering algorithm which starts by selecting the random initial centroids and computes the distance between the centroids and the data objects are computed. The objects are then clustered with the centroids at a minimum distance [4]. The algorithm iteratively groups the data objects with minimum distance until there is no change in the centroid or members of the cluster group. Normalization is used to eliminate redundant data and ensures that good quality clusters are generated which can improve the efficiency of clustering algorithms. So it becomes an essential step before clustering as Euclidean distance is very sensitive to the changes in the differences [5]. A feature weight algorithm can be seen as the combination of a search technique for proposing new feature subsets, along with an evaluation measure which scores the different feature subsets. The simplest algorithm is to test each possible subset of features finding the one which minimizes the error rate. This is an exhaustive search of the space, and is computationally intractable for all but the smallest of feature sets [15].

The remaining sections of the paper are organized as follows: Section 2, review of related works, 3 describes the methodology, section 4 denotes the comparison methods, section 5 explicates the experimental results and finally section 6 explains the conclusion of the proposed work.

2. RELATED WORKS

Zhang Chen *et al.* [6] proposed the initial centroids algorithm based on k-means that have avoided alternative randomness of initial center. Fang Yuan [7] proposed the initial centroids algorithm. The standard k-means algorithm selects k-objects randomly from the given data set as the initial centroids. If different initial values are given for the centroids, the accuracy output by the standard k-means algorithm can be affected. In Yuan's method the initial centroids are calculated systematically. To overcome the efficient k-means clustering method reduces computing efficiency and accuracy when the dataset is increased.

3. METHODOLOGY

3.1 Min-Max Normalization

Min-max normalization [14] performs a linear transformation on the original data. Min-max is a technique that helps to normalize a dataset. It will scale the dataset between the 0 and 1. Suppose that min_A and max_A are the minimum and maximum values of an attribute, A. Min-max normalization maps a value, v , of A to v' in the range $[new_minA, new_maxA]$ by computing

$$v' = \frac{v - minA}{maxA - minA} (new_maxA - new_minA) + new_minA$$

Min-max normalization preserves the relationships among the original data values. It will encounter an “out-of-bounds” error if a future input case for normalization falls outside of the original data range for A.

3.2 Gain Ratio

Information gain applied to attributes that can take on a large number of distinct values might learn the training set too well. The information gain measure is biased toward tests with many outcomes. That is, it prefers to select attributes having a large number of values. The gain ratio [15] is defined as

$$\text{GainRatio (A)} = \frac{\text{Gain(A)}}{\text{SplitInfo(A)}}$$

The attribute with the maximum gain ratio is selected as the splitting attribute. The split information approaches 0, the ratio becomes unstable. A constraint is added to avoid this, whereby

the information gain of the test selected must be large at least as great as the average gain over all tests examined.

3.3 K-Means Clustering Algorithm

The basic idea of K-means algorithm is to classify the dataset D into k different clusters where D is the dataset of n data; k is the number of desired clusters. The algorithm consists of two basic phases [12]. The first phase is to select the initial centroids for each cluster randomly. The second and final phase is to take each point in dataset and assign it to the nearest centroids [12]. To measure the distance between points Euclidean Distance method is used. When a new point is assigned to a cluster the cluster mean is immediately updated by calculating the average of all the points in that cluster [13]. After all the points are included in some clusters the early grouping is done. Now each data object is assigned to a cluster based on closeness with cluster center where closeness is measured by Euclidean distance. This process of assigning a data points to a cluster and updating cluster centroids continues until the convergence criteria is met or the centroids don't differ between two consecutive iterations. Once, a situation is met where centroids don't move any more the algorithm ends. The k-means clustering algorithm is given below.

Step 1: Begin with a decision on the value of k = number of clusters.

Step 2: Put any initial partition that classifies the data into k clusters. You may assign the training samples randomly, or systematically as the following:

1. Take the first k training sample as single-element clusters
2. Assign each of the remaining (N-k) training samples to the cluster with the nearest centroid.

After that each assignment, recomputed the centroid of the gaining cluster.

Step 3: Take each sample in sequence and compute its distance from the centroid of each of the clusters. If a sample is not currently in the cluster with the closest centroid, switch this sample to that cluster and update the centroid of the cluster gaining the new sample and the cluster losing the sample.

Step 4: Repeat step 3 until convergence is achieved, that is until a pass through the training sample causes no new assignments.

3.4 Proposed Methodology

The proposed efficient k-means clustering is upgraded the origin k-means clustering to reduce the computational complexity. In the proposed efficient k-means clustering method, the normalization and feature weight are applied. Firstly, the methodology employs normalized dataset by using min-max normalization to improve the efficiency of clustering algorithm. After that gain ratio method compute feature weights for each attributes of the data to minimize the error rate. It the centroids are then posted to the traditional clustering algorithms for being executed in the way it normally does. The results of the proposed work are validated against number of iterations and accuracy obtained and compared with the randomly selected initial centroids.

Step 1: Accept the dataset to cluster as input values

Step 2: Perform a linear transformation on the original dataset using mix-max normalization

Step 3: Compute the feature weight for each attribute and update the dataset.

Step 4: Initialize the first K cluster

Step 5: Calculate centroid point of each cluster formed in the dataset.

Step 6: Assign each record in the dataset for only one of the initial cluster using a measure Euclidean distance.

Step 7: Repeat step 4 until convergence is achieved, that is until a pass through the training sample causes no new assignments.

4. COMPARISON METHODS

4.1 Normalized Mutual Information (NMI)

The normalized mutual information [11] is a good measure for determining the quality of clustering. Comparing the NMI between different clustering, having different number of clusters the proposed efficient k-means clustering can be measured. The value of NMI is large, the cluster quality is good.

$$NMI(Y, C) = \frac{2 \times I(Y, C)}{[H(Y) + H(C)]}$$

4.2 Silhouette Coefficient (SC)

The silhouette coefficient [9] is used to compare the quality of clustering for origin k-means and proposed method. The cluster quality is good, when the value of SC is large.

$$SC = \frac{1}{N} \sum_{i=1}^N s(x)$$

$$s(x) = \frac{b(x) - a(x)}{\max\{a(x), b(x)\}}$$

4.3 Sum of Square Error (SSE)

The sum of square error [10] is defined to use measure the quality of clustering that is the difference of error between the original k-means and proposed method. The value of SSE is small, the cluster quality is good.

$$SSE = \sum_{i=1}^K \sum_{x \in C_i} dist2(mi, x)$$

5. EXPERIMENTAL RESULTS

In this section, we use Iris [8] dataset to validate the proposed algorithm. The performance of our proposed algorithm is examined in the quality of clustering required with different real world dataset and compared with the origin k-means algorithm.

In Table 1 and Figure 1 shows the comparison of proposed algorithm and k-means with the quality of clustering for cluster two.

Table 1. Evaluation result of Iris data for the quality of clustering, k = 2

Number of Clusters	Method	Normalized Mutual Information (NMI)	Silhouette Coefficient (SC)	Sum of Square Error (SSE)
K = 2	K-Means	0.6565	0.7813	0.9077

	Proposed	0.6565	0.8149	0.0047
--	----------	--------	--------	--------

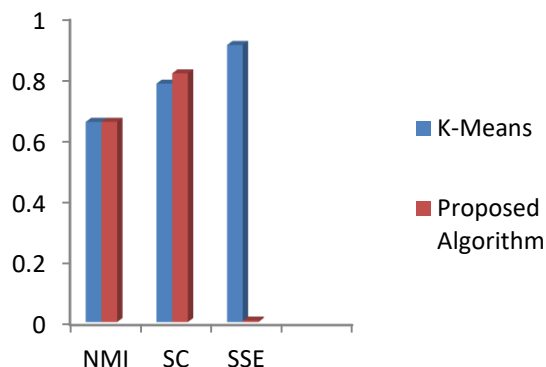


Figure 1. The quality of clustering for cluster 2

The comparison of proposed algorithm and k-means with the quality of clustering for cluster three. The result is shown in Figure 2 and Table 2.

Table 2. Evaluation result of Iris data for the quality of clustering, k = 3

Number of Clusters	Method	Normalized Mutual Information (NMI)	Silhouette Coefficient (SC)	Sum of Square Error (SSE)
K = 3	K-Means	0.7419	0.8149	0.5281
	Proposed	0.8642	0.8515	0.0023

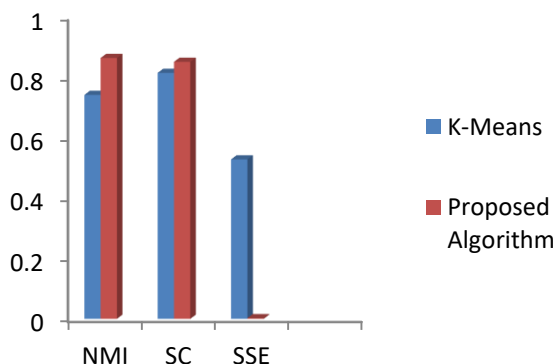


Figure 2. The quality of clustering for cluster 3

In Table 3 and Figure 3 shows the comparison of proposed algorithm and k-means with the quality of clustering for cluster four.

Table 3. Evaluation result of Iris data for the quality of clustering, k = 4

Number of Clusters	Method	Normalized Mutual Information (NMI)	Silhouette Coefficient (SC)	Sum of Square Error (SSE)
K = 4	K-Means	0.7006	0.681	0.409
	Proposed	0.8	0.9141	0.0019

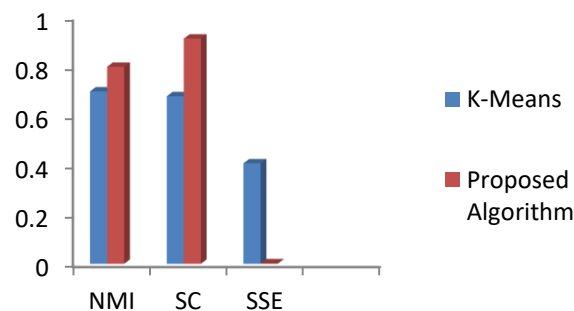


Figure 3. The quality of clustering for cluster 4

The comparison of proposed algorithm and k-means with the quality of clustering for cluster five. The result is shown in Figure 4 and Table 4.

Table 4. Evaluation result of Iris data for the quality of clustering, k = 5

Number of Clusters	Method	Normalized Mutual Information (NMI)	Silhouette Coefficient (SC)	Sum of Square Error (SSE)
K = 5	K-Means	0.6939	0.6591	0.3167
	Proposed	0.7036	0.5604	0.0015

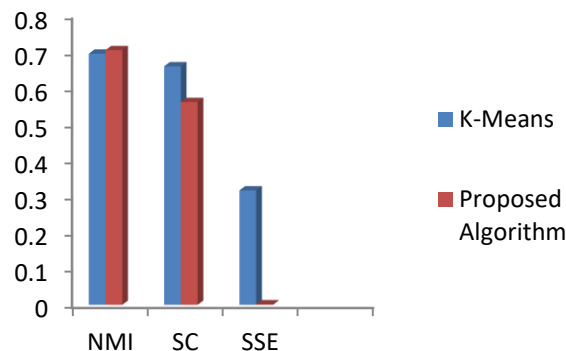


Figure 4. The quality of clustering for cluster 5

6. CONCLUSIONS

K-means is good clustering algorithm but k-means algorithm does not always generate good quality results as automatic initialization of centroids affects final clusters. The proposed algorithm is found to be more accurate and efficient compared to the original k-means algorithm. This proposed method finding the better initial centroids and provides an efficient way of assigning the data to the suitable clusters. The computational complexity of the standard k-means algorithm is high than this proposed k-means algorithm. This system is done by assigning weights to each attribute value to achieve standardization. This algorithm has proved to be better than standard k-means algorithm in terms of cluster quality.

7. REFERENCE

- [1] Vaishali R. Patel, Rupa G. Mehta, “Impact of Outlier Removal and Normalization Approach in Modified k-Means Clustering Algorithm”, IJCSI International Journal of Computer Science Issues, Vol. 8, Issue 5, No 2, 2011, pp. 331-336.
- [2] R. Agrawal, T. Imielinski and A. Swami, “Mining association rules between sets of items in large database”, The ACM SIGMOD Conference, Washington DC, USA, 1993, pp. 207-216.
- [3] David Arthur & Sergei Vassilvitskii , "How Slow is the k means Method?", Proceedings of the 22nd Symposium on Computational Geometry (SoCG), 2006, pp. 144-153.
- [4] A. Joy Christy, S. Hari Ganesh, “Building Numerical Clusters Using Multidimensional Spherical Equation”, International Journal of Applied Engineering Research, ISSN 0973-4562, Volume 10, Issue No.82, pp:629-634, 2015.
- [5] Md Sohrab Mahmud, Md. Mostafizer Rahman, Md. Nasim Akhtar, “Improvement of K-means Clustering algorithm with better initial centroids based on weighted average”, 7th International Conference on Electrical and Computer Engineering, 2012, pp. 647-650.
- [6] Chen Zhang and Shixiong Xia, K-means 2009. Clustering Algorithm with Improved Initial center, in Second International Workshop on Knowledge Discovery and Data Mining (WKDD), pp: 790-792.
- [7] Yuan, F., Z.H. Meng, H.X. Zhangz, C.R. Dong, August 2004. A New Algorithm to Get the Initial Centroids, proceedings of the 3rd International Conference on Machine Learning and Cybernetics, pp: 26-29.
- [8] 2010. The UCI Repository website [Online]. Available: <http://archive.ics.edu/>
- [9] Rousseeuw, P. J. (1987). Silhouettes: a graphical aid to the interpretation and validation of cluster analysis. Journal of Computational and Applied Mathematics. Vol.20, pp.53-65.
- [10] Kwedlo, W. (2011). A clustering method combining differential evolution with the k-means algorithm. Pattern Recognition Letters. Vol.32, pp.1613–1621.
- [11] F. Knops, Zeger & B. Antoine Maintz, J & A. Viergever, Max & P. W. Pluim, Josien. (2003). Normalized Mutual Information Based PET-MR Registration Using K-Means Clustering and Shading Correction. 2717. 31-39.
- [12] J. Han and M. Kamber, Data Mining Concepts and Techniques, Morgan Kaufmann Publishers, San Diego, 2001.
- [13] Margaret H. Dunham, Data Mining-Introductory and Advanced Concepts, Pearson Education, 2006
- [14] Navdeep Kaur and Krishan Kumar, “Normalization Based K-means Data Analysis Algorithm”, International Journal of Advanced Research in Computer Science and Software Engineering, ISSN: 2277 128X, Volume 6, Issue, June 2016, pp. 455-457
- [15] R. Praveena Priyadarsini, M.L.Valarmathi and S. Sivakumari, “Gain Ratio Based Feature Selection Method For Privacy”, ICTACT Journal on Soft Computing, April 2011, Volume: 01, Issue: 04, pp. 201-205

Seismic Performance Evaluation of Knee and EBF Braced Frames Using Nonlinear Static Analysis

Amin Moshtagh
Assistant Professor
Civil Engineering Department
Garmsar University
Garmsar City, Semnan, Iran

Vahid Saberi
Assistant professor
Civil Engineering Department
Eyvanekey University
Eyvanekey City, Semnan, Iran

Hamid Saberi
Assistant professor
Civil Engineering Department
Eyvanekey University
Eyvanekey City, Semnan, Iran

Abstract: Earthquake-resistant structure systems should be designed to stand large deformation to absorb and attenuate imposed energy due to an earthquake while providing sufficient stiffness to transfer the forces to the base without collapse. Knee Braced Frames (KBF), which involves added additional diagonal elements to a frame to increase its ability to withstand lateral loads, is suggested by several researches. In this study, the seismic performance of KBFs are evaluated and compared with Eccentric Braced Frames (EBF). Nonlinear static analyses were utilized for seismic evaluation and comparison between the mentioned frame systems. Three steel structures of 5, 10, and 15-story were numerically modeled, and the seismic parameters such as lateral stiffness, inter-story drift, ductility, and response modification factors were calculated for each structure system. It was observed that using KBF systems resulted in a reduction in intersotry drifts compared to EBFs. KBF systems show more stiff responses in comparison with EBFs and they presented much more stiff response by reducing the knee element length. The KBFs have more ductile behavior in comparison with EBFs, although base shear in KBFs is less than EBFs.

Keywords: EBF Bracing, Knee Bracing, Nonlinear Analysis, Pushover, Seismic Parameters

1. INTRODUCTION

Earthquake-resistant structures should be designed in a way that they are able to stand against large deformation due to the earthquake to absorb and attenuate imposed energy. On the other hand, they should have a sufficient stiffness for transferring the forces to base without collapse. To fulfill these goals, using bracing system which involves added diagonal elements to a frame to increase its ability to withstand lateral loads is an option. There are two major braced frame systems, Concentric Braced Frame (CBF) and Eccentric Braced Frame (EBF). CBFs consist of diagonal braces located in the plane of the frame where both ends of the brace connected to the ends of other framing members while for EBF system one or both ends of the brace do not connected to the ends of other framing members. In the CBF systems, members form a truss-like structure, creating a stiff frame while EBF combines the features of a moment frame and a concentrically braced frame and minimizing the disadvantages of each system resulting to improve in the system performance in the event of earthquakes.

Although EBFs usually have appropriate behavior, after the failure of the link beam (the element between two ends of the brace in the floor), floor beam would be seriously damaged. Since this element is considered as one of the main structural components, structural rehabilitation would be difficult and sometimes impossible. Moreover, bracing elements and shear links dissipate energy when exposed to the strong earthquakes, but in the weak earthquake, link beam would stay in the elastic region. In addition, analysis and design of link beams are complex. Therefore, attempts for finding seismic resistant systems with large ductility and stiffness have been continued. These drawbacks are mitigated to some extent in the works of Aristizabel-Ochoa in 1986 by introducing Disposable Knee Bracing systems as a new alternative structural system for earthquake-resistant steel

structures [1]. This system possesses an appropriate stiffness and absorbs earthquake energy through yielding of knee elements. In addition, the diagonal element provides lateral stiffness during moderate earthquakes. However, the knee element is designed to behave in nonlinearity range for dissipation of the energy under strong ground motions.

Many researches have been performed to study the experimental and analytical performance of knee brace systems. Sam et al. 1995 carried out pseudo dynamic testing of 1-story and 2-story specimens using KBF system, which showed the system has enough capacity to reduce the earthquake damage effectively and economically [2]. Maheri et al. 2003 performed pushover testing of KBF and CBF systems mounted on concrete reinforced moment resisting frame structures. The response modification factors of the systems are evaluated and significant improvement in the ductile behavior was observed in the contract of unbraced reinforced concrete building [3].

In this study, the seismic performance of KBF systems is evaluated and compared with EBF systems. Nonlinear static analyses were utilized for seismic evaluation and comparison between the mentioned frame systems. Three steel structures of 5-story, 10-story, and 15-story were modeled numerically, and the seismic parameters such as lateral stiffness, ductility, and response modification factors were calculated for each structure system.

2. STRUCTURE DESIGN

Seismic and gravity loads applied to the structures according to ASCE 7-10 [4]. For calculating static equivalent lateral load, it was assumed that the buildings were located in a high seismic region, and soil type C was selected. Response modification factors for EBF and KBF systems are assumed to be 7. Dead and live loads are 700 and 200 kg/m^2 , respectively. Design of the structures was performed

according to load and resistance factor design method (LRFD) of AISC 2010 [5].

3. STRUCTURE CONFIGURATIONS

In knee braces, the optimum knee element is defined when the frame has the highest stiffness. In another word, according to Fig. 1 $b/B=h/H$ i.e. knee element is parallel to the diagonal frame and element extension passes through the intersection between beam and column. The frames have five, four, and three spans, and all span widths equal to 7 m. The frames have 5, 10, 15-story and each story height is 3.2 m. Lengths of the link beams and knees in the frames are variable. Box sections and plate girders are utilized for designing the columns and beams. In addition double U-sections were used for the braces. Small boxes were also considered for designing the knee elements. The connections between the beams and columns were assumed to be pinned.

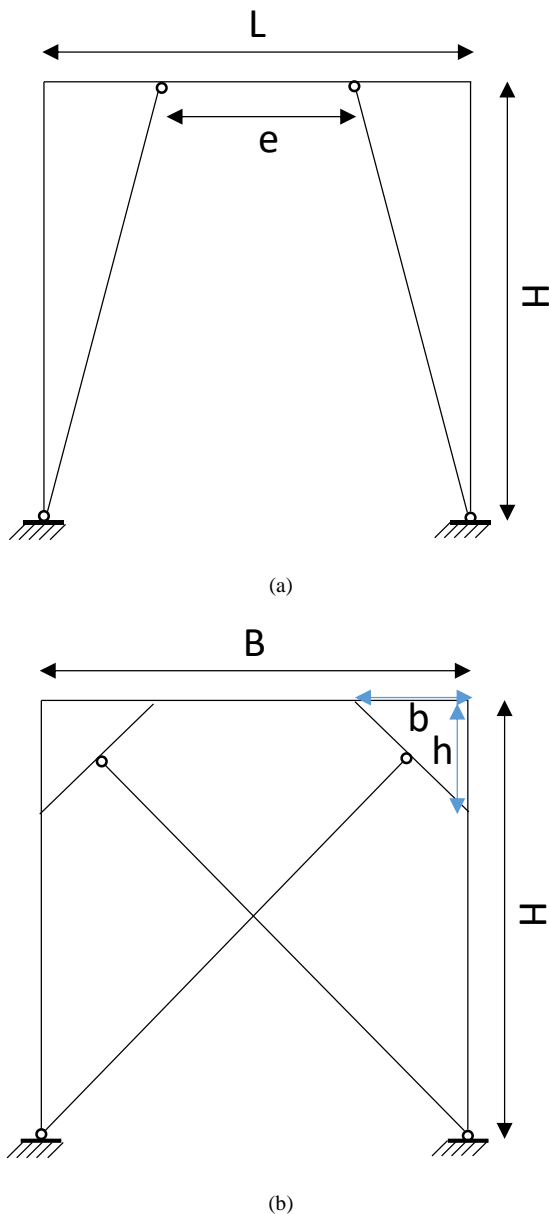


Fig. 1: Sample frame: (a) EBF, and (b) Knee braced frame.

4. NONLINEAR STATIC ANALYSIS

Nonlinear static analysis (pushover analysis) are now widely used in engineering practice to estimate seismic parameters in building structures. Pushover analysis has been utilized [6-9] for seismic demand and parameter estimation of structures. For instance, Taghinezhad et al used pushover analysis to predict amplification factor, inter-story drift and seismic vulnerability in different structure systems [8]. In this method, the lateral load is statically applied to the structures, and continuously increased until the roof displacement in a specific point (control point) reaches target displacement, which is defined according to the following equation:

$$\delta_t = C_0 C_1 C_2 C_3 S_a \frac{T_e^2}{4\pi} g \quad (1)$$

Where T_e is an effective fundamental period of building in a specific direction. S_a is spectrum acceleration corresponding to T_e . C_0 , C_1 , C_2 , and C_3 are the modification factors.

In this study two lateral load pattern were applied to the structures:

1. First lateral load pattern was according to the first vibrational mode of the structure.
2. Second lateral load pattern was uniform load according to the story weights based on Eq. (2):

$$F_i = \frac{W}{\sum_{j=1}^n W_j} V \quad (2)$$

Where F_i is applied force for each story, W_i is weight for i -th story, and V is base shear force. Plastic hinge properties were defined according to FEMA 356 [10].

5. ELASTIC FRAME STIFFNESS

Stiffness of frames derived from equivalent bilinear form of capacity curves resulted from pushover analysis and presented in Fig. 2 in terms of h/H and e/L for EBF and KBF systems, for 5-story, 10-story, and 15-story frames. It is observed that using KBF increases the stiffness of braced frames. This difference is higher for lower values of h/H and e/L .

6. SEISMIC PARAMETERS

By using force-displacement curves of the frames, seismic parameters such as ductility, response modification, and over strength factors can be estimated. In addition, plastic hinge formation of the structures can be evaluated [11]. There are two analytical methods for estimating the capacity curve of a structure (force-displacement curve); using nonlinear static and incremental dynamic analysis. In incremental dynamic analysis, capacity curves of a structure is estimated by applying several earthquakes with incremental scale factors considering the nonlinear phase of structure material. Several researches utilized [12-17] this numerical method to estimate the seismic parameters. Soltangharai et al, 2015 and 2016, [12, 15] estimated the seismic parameters of steel buckling restrained and steel moment restrained frames using incremental dynamic analysis with considering the near-fault

or far-fault earthquake effects. In this study nonlinear static analysis [18-23] was employed to estimate the capacity curves of the structures. In pushover analysis, the nonlinear phase of the structure is considered and lateral load is incrementally increased according to the defined load pattern to capture the real response of the structure under extreme seismic loads [22-24].

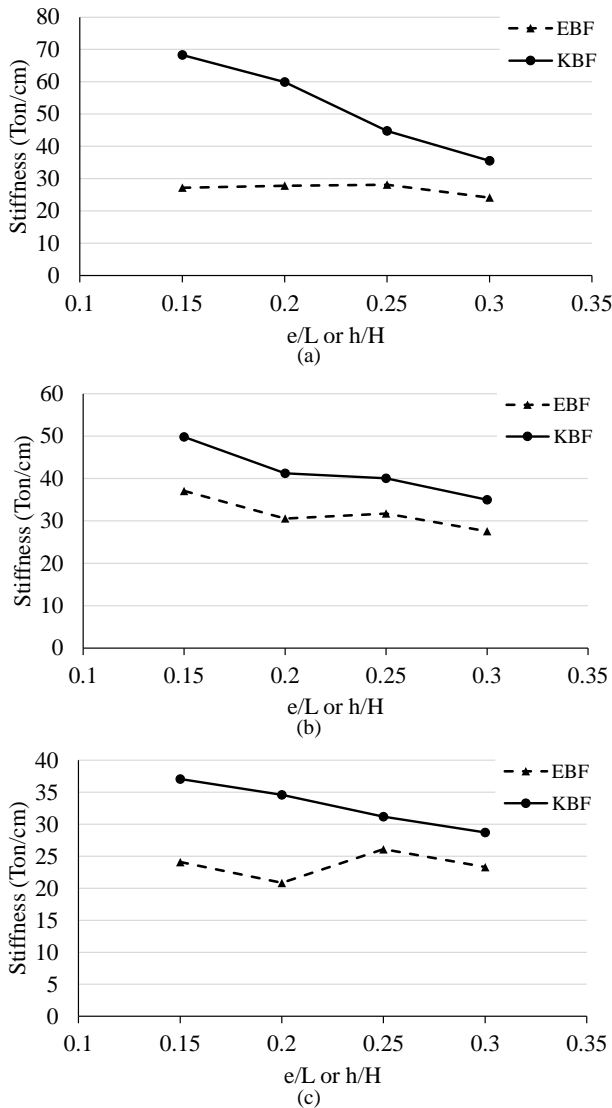


Fig. 2: Frame lateral stiffness: (a) 5-story, (b) 10-story, and (c) 15-

story.

This response modification factor is the ratio of yield shear force (V_y) based on bilinear form of capacity curve and corresponding force of first plastic hinge formation (V_s), which is denoted by R_{so} or Ω_0 .

$$R_{so} = \frac{V_y}{V_s} \quad (3)$$

The other equations are:

$$R_s = R_{so} \times F_1 \times F_2 \times \dots \quad (4)$$

$$R = R_s \times R_\mu \quad (5)$$

Where R_u is response modification factor based on ultimate strength stress, and R_w is response modification factor based on allowable stress design. The ratio of response modification factors between these two design methods is:

$$Y = R_w / R_u \quad (6)$$

Y depends on different design provision ranging from 1.4 to 1.7.

Different equations have been proposed for estimating ductility reduction factor (R_μ). One of the comprehensive equation has been proposed by Miranda. His equation includes the effect of fundamental period of structure, soil type, and earthquake ground acceleration [25-28].

$$R_\mu = \frac{\mu - 1}{\phi} + 1 \quad (7)$$

For hard rock type:

$$\phi = 1 + \frac{1}{10T - \mu T} - \frac{1}{2T} \exp \left[-3/2 \left(\ln T - \frac{3}{5} \right)^2 \right] \quad (8)$$

Table 1: Seismic parameters of EBF structures.

Structure	T_e (sec)	V_y (ton)	V_s (ton)	R_{so}	R_s	μ	ϕ	R_μ	R_u	R_w
5-story	0.80	290	249	1.16	1.34	2.51	0.78	2.92	3.92	5.48
10-story	1.23	572	388	1.47	1.70	2.10	0.76	2.45	4.15	5.81
15-story	1.88	972	572	1.70	1.95	2.21	0.91	2.33	4.55	6.64

Table 2: Seismic parameters of KBF structures.

Structure	T_e (sec)	V_y (ton)	V_s (ton)	R_{so}	R_s	μ	ϕ	R_μ	R_u	R_w
5-story	0.63	178	112	1.59	1.83	3.84	0.93	4.05	7.40	10.36
10-story	1.03	315	265	1.19	1.37	3.76	0.75	4.67	6.39	8.95
15-story	1.72	577	356	1.62	1.86	3.14	0.88	3.43	6.39	8.93

For stiff soil type:

$$\phi = 1 + \frac{1}{12T - \mu T} - \frac{2}{5T} \exp\left[-2\left(\ln T - \frac{1}{5}\right)^2\right] \quad (9)$$

For soft clay type:

$$\phi = 1 + \frac{T_g}{3T} - \frac{3T_g}{4T} \exp\left[-3\left(\ln \frac{T}{T_g} - \frac{1}{4}\right)^2\right] \quad (10)$$

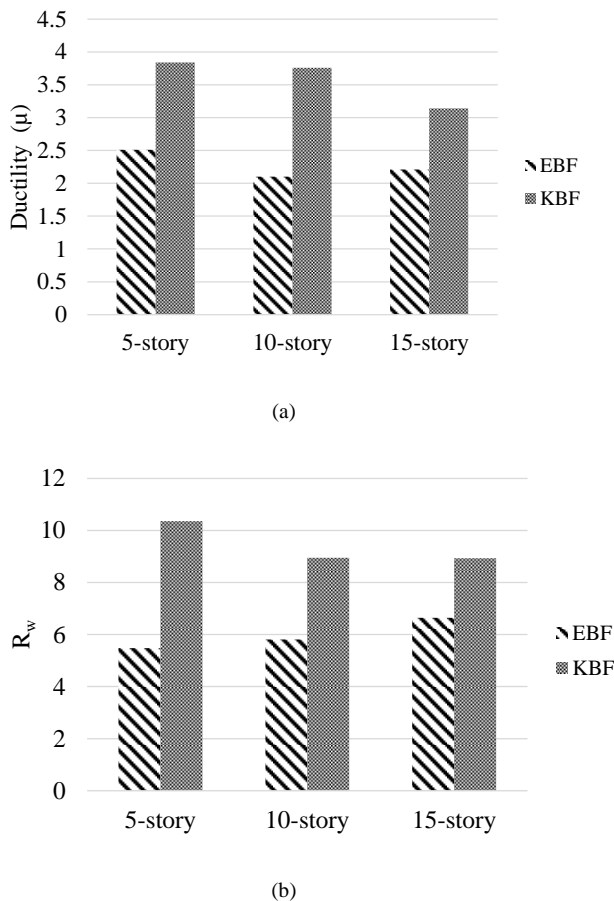


Fig. 3: (a) Ductility and (b) response modification factor for EBF and KBF.

Response modification and ductility factors for EBF and KBF for $h/H=e/L=0.3$ are presented in Table 1 and 2, respectively.

According to the Tables 1 and 2, it can be observed that response modification factors for KBF range 8.5 to 10.5; whereas the values for EBFs are much less than them. Furthermore, the ductility values for KBFs are more than EBFs.

It is observed from Fig. 3 that the calculated response modification factors and ductility of KBF system is more than the values of EBFs. Therefore, as expected, KBF systems can provide higher ductility compared to EBFs.

According to Fig. 4, it is shown that base shears in the target displacements for KBFs are more than EBFs, and this

difference increases for the frames with larger story numbers. In addition, stiffness for EBFs is larger than for EBF systems.

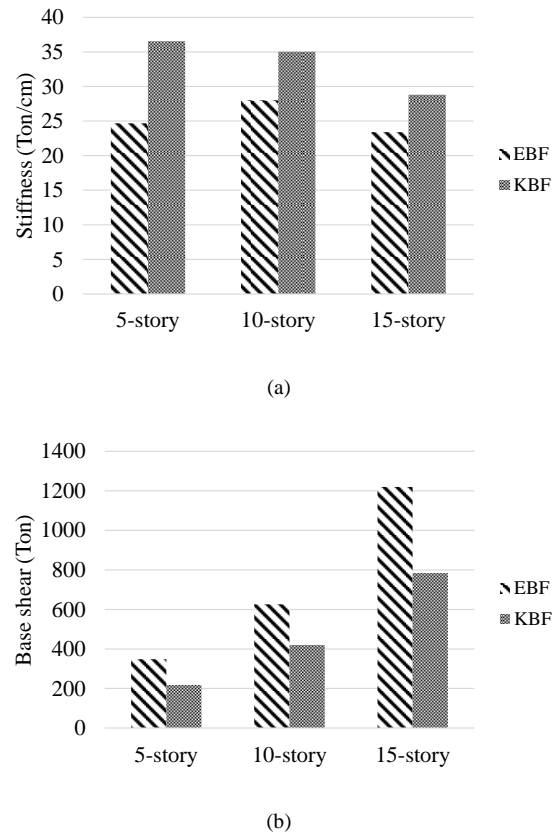


Fig. 4: (a) Stiffness, and (b) Base shear for EBF and KBF.

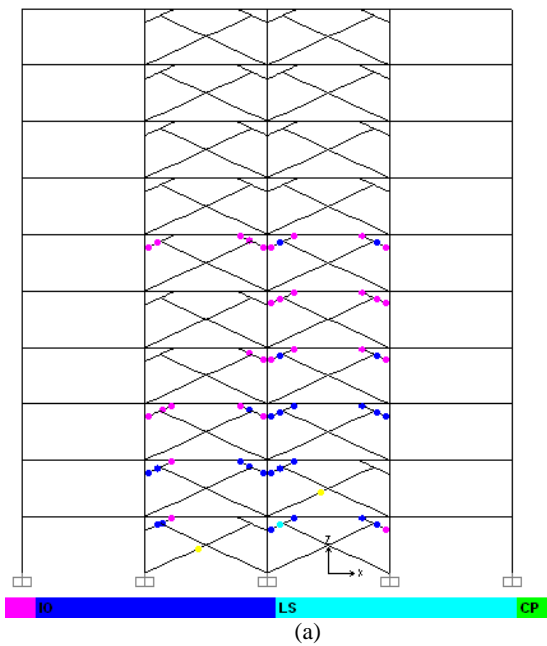
7. NONLINEAR PERFORMANCE OF FRAMES:

Plastic hinge distribution for the KBF and EBF 10-story structure resulted from nonlinear static analyses is shown in Fig. 5.

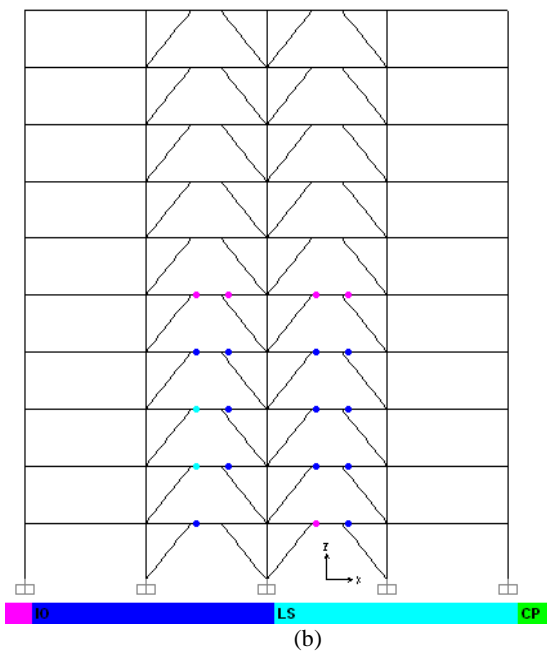
It is observed that first hinge was formed in the knee elements for KBF system. Knee element is considered as a secondary or fuse element in the lateral resistant system, which can be repaired or replaced easily after a server earthquake. On the other hand, plastic hinges generally started to form in links between two ends of braces, which are the main structural element to dissipate energy, in EBF systems. The produced damages in the links of EBF systems can be very expensive to repair.

8. INTER-STORY DRIFT

According to seismic design codes, one of the significant parameters, which should be considered for seismic designing, is inter-story drift. The inter-story drifts for knee braced frames are less than eccentrically braced frames as shown in Fig. 6.

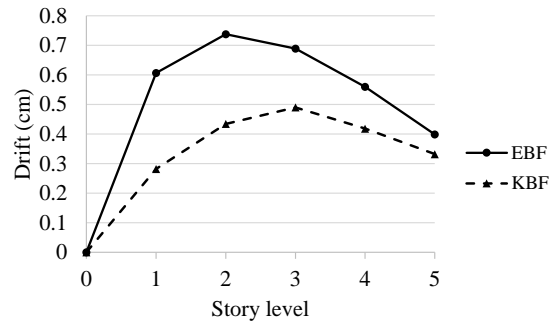


(a)

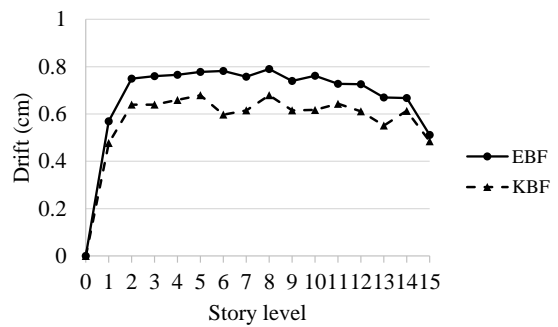


(b)

Fig. 5: Plastic hinge distribution for: (a) KBF, and (b) EBF.



(a)



(b)

Fig. 6: Inter-story drift for: (a) 5-story, and (b) 15-story frames.

9. CONCLUSION

In this study, the seismic performance of KBFs and EBFs was evaluated, and the following conclusions were made:

1. Using KBF system causes a reduction in inter-story drifts compared to EBFs;
2. Comparing the two similar EBFs and KBFs (identical story number and span length), it is shown that KBFs are stiffer than EBFs. KBFs become much stiffer by reduction of knee element length;
3. Retrofit and maintenance of KBF system is less expensive and more constructible than EBF due to nonlinearity in knee element which is a secondary element in comparison with link beam in EBFs which is a primary structural element;
4. Ductility of KBFs are more than EBFs, although base shear in KBFs is less than EBFs.

10. REFERENCE

- [1] J.D. Aristizabal-Ochoa, Disposable knee bracing: improvement in seismic design of steel frames. *Journal of Structural Engineering*, 112(7), 1986, 1544-1552.
- [2] M. Sam, T. Balendra, and C. Liaw, Earthquake resistant steel frames with energy dissipating knee elements, *Journal of Engineering Structures*, 17(5), 1995, 334–343.

- [3] M.R. Maheri, R. Kousari, and M. Razazan, Pushover tests on steel X-braced and knee-braced RC frames, *Journal of Engineering Structures*, 25(13), 2003, 1697–1705.
- [4] ASCE/SEI 7-10, *Minimum design loads for buildings and other structures*, American Society of Civil Engineers, Reston, Virginia, 2010.
- [5] ANSI/AISC 360-16, *Specification for structural steel buildings*. American Institute of Steel Construction, Chicago, Illinois, 2016.
- [6] A.K. Chopra, and R.K. Goel, A modal pushover analysis procedure for estimating seismic demands for buildings. *Earthquake Engineering and Structural dynamics*, 31(3), 2002, 561-582.
- [7] H. Krawinkler, and G.D.P.K. Seneviratna, Pros and cons of a pushover analysis of seismic performance evaluation. *Engineering Structures*, 20(4-6), 1998, 452-464.
- [8] R. Taghinezhad, A. Taghinezhad, V. MahdaviFar, and V. Soltangharai, Evaluation of story drift under pushover analysis in reinforced concrete moment frames, *International Journal of Research and Engineering*, 5(1), 2018, 296-302.
- [9] T.S. Paraskeva, A.J. Kappos, and A.G. Sextos, Extension of modal pushover analysis to seismic assessment of bridges. *Earthquake Engineering and Structural Dynamics*, 35(10), 2006, 1269-1293.
- [10] FEMA 356, *Pre-standard and commentary for the seismic rehabilitation of buildings*, Washington, DC, 2000.
- [11] A.A. Nassar, J.D. Osteras, and H. Krawinkler, Seismic design based on strength and ductility demands. *Proc. 10th World Conference on Earthquake Engineering*, 1992, 5861-5866.
- [12] V. Soltangharai, M. Razi, and M. Gerami, Comparative evaluation of behavior factor of SMRF structures for near and far fault ground motions. *Periodica Polytechnica Civil Engineering*, 60(1), 2016, 75-82.
- [13] N. Fanaie, and S. Ezzatshoar, Studying the seismic behavior of gate braced frames by incremental dynamic analysis (IDA). *Journal of Constructional Steel Research*, 99, 2014, 111-120.
- [14] B. Asgarian, and H.R. Shokrgozar, BRBF Response modification factor. *Journal of Constructional Steel Research*, 65(2), 2009, 290-298.
- [15] V. Soltangharai, M., Razi, and M. Gerami, Behaviour factor of buckling restrained braced structures for near and far fault ground motions. *International Journal of Structural Engineering*, 6(2), 2015, 158-171.
- [16] A. Kheyroddin, and N. and Mashhadiali, Response modification factor of concentrically braced frames with hexagonal pattern of braces. *Journal of Constructional Steel Research*, 148, 2018, 658-668.
- [17] M. Mahmoudi, and M.G. Abdi, Evaluating response modification factors of TADAS frames. *Journal of Constructional Steel Research*, 71, 2012, 162-170.
- [18] M. Izadinia, M.A., Rahgozar, and O. Mohammadrezaei, Response modification factor for steel moment-resisting frames by different pushover analysis methods. *Journal of Constructional Steel Research*, 79, 2012, 83-90.
- [19] F.R. Rofooei, and M.R. Mirjalili, Dynamic-based pushover analysis for one-way plan-asymmetric buildings. *Engineering Structures*, 163, 2018, 332-346.
- [20] J. Kim, and H. Choi, Response modification factors of chevron-braced frames. *Engineering structures*, 27(2), 2005, 285-300.
- [21] M. Mahmoudi, and M. Zaree, Determination the response modification factors of buckling restrained braced frames, *Procedia Engineering*, 54, 2013, 222-231.
- [22] R. Taghinezhadbilondy, A. Yakel, and A. Azizinamini, Deck-pier connection detail for the simple for dead load and continuous for live load bridge system in seismic regions, *Engineering Structures*, 173(15), 2018, 76-88.
- [23] R. Taghinezhadbilondy, *Extending use of simple for dead load and continuous for live load (SDCL) steel bridge system to seismic areas. doctoral diss.*, Florida International University, Miami, FL, 2016
- [24] V. MahdaviFar, A. Sinha, A.R. Barbosa, L. Muszynski, and R. Gupta, Lateral and withdrawal capacity of fasteners on hybrid cross-laminated timber panels. *Journal of Materials in Civil Engineering*, 30(9), 2018, 04018226.
- [25] V. MahdaviFar, A.R. Barbosa, A. Sinha, L. Muszynski, R. Gupta, S. E. Pryor, Hysteretic Response of Metal Connections on Hybrid Cross-Laminated Timber Panels. *Journal of Structural Engineering*, 145(1), 2018, 04018237.
- [26] R.L. Wood, D.T. Gillins, M.F. Mohammadi, F. Javadnejad, H. Tahami, M.N. Gillins, and Y. Liao, 2015 Gorkha post-earthquake reconnaissance of a historic village with micro unmanned aerial systems. Proc. 16th World Conference on Earthquake, Tokyo, Japan, 2017.
- [27] E. Miranda, and V.V. Bertero, Evaluation of strength reduction factors for earthquake-resistant design. *Earthquake Spectra*, 10(2), 1994, 357–379.
- [28] V. MahdaviFar, "Cyclic performance of connections used in hybrid cross-laminated timber." Ph.D. Dissertation, 2017, Oregon State University.

Design and Numerical Stress Analysis of Spur Gear (Power Tiller)

Aye Nwe Moe
Department of Mechanical
Engineering
Technological University
(Thanlyin), Myanmar

Khin Khin Htar
Department of Mechanical
Engineering
Yangon Technological University
Myanmar

Khin Swe Swe Latt
Department of Mechanical
Engineering
Technological University
(Thanlyin), Myanmar

Abstract: This paper deals with the design and stress analysis of spur gear of GT-1 Power Tiller (Global Tiller-1). It is widely used in Myanmar because they are more efficient and cheaper than any others types of tractors for agricultural works. The fundamental dimensions of engine are four strokes with compression ratio of 22.5. It produces maximum rated output power of 15 hp at 2400 rpm and maximum speed 24.2 km/hr at 2400 rpm. In gear design, gear material is chosen Carbon Steel (AISI 5160 OQT 400) and all gear are the same material. The gears are designed to transmit power and satisfy the dynamic check. In gear design, the number of teeth, face width, gear tooth features and pitch diameter are calculated. Three-dimensional model of Spur gear is drawn by using SolidWorks Software and analysed by Finite element method. The spur gears are designed according to the point of view of the strength. The result of spur gear design and stress depend upon the tooth profile and gear material properties. The spur gear is analysed with Carbon Steel (AISI 5160 OQT 400). Boundary constraints are defined and the deflection and strain for three-dimensional model are analysed.

Keywords: Spur Gear, Face Width, 3D model, Dynamic Check, SolidWorks

1. INTRODUCTION

Myanmar is an agricultural country and 85percent of Myanmar are farmers. Therefore, Government of Myanmar is always helping the farmers in various ways, it has distributed interest free agricultural loans to farmers, sold chemical fertilizer and farm implements to farmers cheaply, built dams and irrigation channels all over the country, taught modern methods of farming to farmers and helping them to have double cropping and mixed cropping.

Food is necessary for human being from many years ago to nowadays people do farming for this food, clothes and shelter all mankind is depended on this industry, and everyone is fundamentally concerned with its welfare. Agricultural engineering is the application of any and all branches of engineering to the extent that they may be used in farming, in rural living, rural processing of farm products.

Designer and technicians must design the machine and equipment to meet required standards. Every farm equipment and machine must be adaptable for required standard. There are many kinds of farm tractors such as LY-16 Power Tiller, Dongfeng Power Tiller, GT-1 Power Tiller, etc. Nowadays, Power Tillers are widely used in Myanmar because they are more efficient and cheaper than any others types of tractors for agricultural works. It can be used in various types of farm operations such as ploughing, harrowing, transporting and etc. In this thesis, one of the most important components of Power Tiller that is the gearbox.

To develop Myanmar's agriculture, Power Tillers are important from other country. But sometimes and in some where these Power Tiller and their components of Myanmar's agricultural and environmental conditions. Moreover, the gearboxes of power tiller are found. Therefore, some design of this gearbox is necessary. Therefore, in this paper 'Stress Analysis of Spur Gear' is presented. GT-1 Power Tiller is designed and constructed by Agricultural Mechanization Department for pulling and may be equipped with the diesel engine. It featured by compactness and simplicity in

construction, easy operation and transferring, high durability, reliability and adaptability. The Power Tiller is equipped with riding installation for operations, so as to lighten the driver's degree of fatigue and raise its labor productivity, suit for paddy and dry field. It can be used not only as a transport vehicle with a trailer but also for primary and secondary tillage operations and harvesting of paddy and crops. Power Tiller is composed with many material parts and following Figure shows the main component of Power Tiller.

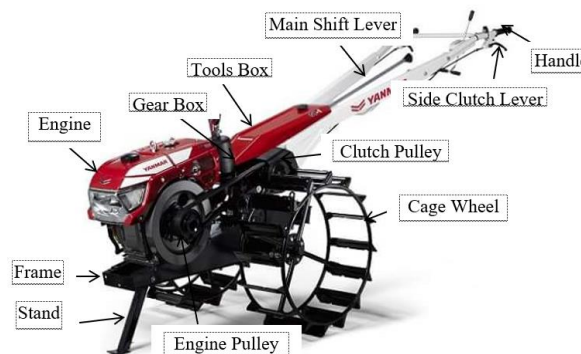


Figure 1. Components of Power Tiller

2. SPECIFICATION AND DESIGN CALCULATION

The design theory and calculation of transmission are mostly dependent upon the maximum torque of the input speed from the engine. In the gearbox, the components are housing, shafts, bearings, gears, shift fork mechanisms. In this paper, the design and stress analysis of spur gears are described. Gears are widely used for transmitting small or large amounts of power from one shaft to another. They operate by direct contact of one body upon the other and maintain a constant velocity ratio between the two shafts. Various types of gearing have been developed for this purpose which will operate

quietly and with very low friction losses. Gears can be classified according to the natural position of shafts. Gears have the advantages of providing positive drive without slip and permit high torque to be transmitted. Gears can be used between shafts, which can be parallel or inclined to one another. Spur gears are toothed wheels whose tooth elements are straight and parallel to the shaft axis; they are used to transmit motion and power between parallel shafts. Figure 2 shows the spur gear pair.

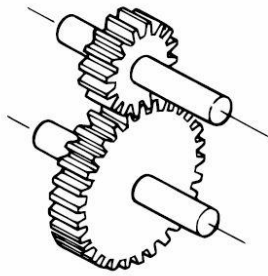


Figure 2. Spur Gear Pair

The design consideration and calculation of transmission are mostly dependent upon the maximum torque of the input speed from the engine. In gear design, Gear material is Carbon Steel (AISI 5160 OQT 400), all gear is the same material. To design the gearbox of power tiller, the required data are collected from the existing transmission.

Model GT-1(Global Tiller-1)

Overall length	3055 mm
Overall width	1205 mm
Overall height	1225 mm
Overall weight	365 kg
Ground clearance	295 mm
Maximum speed	24.2 km / h
Compression ratio	22.5: 1
Max: power	15hp at 2400 rpm
Main clutch type	dry multi-disc clutch
Transmission	3 speed manual

Engine specification horizontal single cylinder - 4 stroke Diesel engine

Design Calculation of First Gears (Unknown Diameter Case)

$$\text{Addendum} = 0.8 m = 0.8 \times 2.5 = 2 \text{ mm}$$

$$\text{Dedendum} = 1 m = 1 \times 2.5 = 2.5 \text{ mm}$$

$$\text{Whole depth} = 1.8 m = 1.8 \times 2.5 = 4.5 \text{ mm}$$

$$\text{Minimum clearance} = 0.2 m = 0.5 \text{ mm}$$

When two gear mesh, the smaller gear is called the pinion and larger is gear. Profile angle selected 20 deg stub involute.

Number of teeth of pinion, $n_p = 17$ teeth

Number of teeth of gear, $n_g = 40$ teeth

$$\text{Design Engine Power} = 15 \text{ hp} \times \frac{0.74596 \text{ kW}}{1 \text{ hp}} = 11.185 \text{ kW}$$

Rated Engine Speed = 2400 rpm

Diameter of engine pulley = 90.5 mm

Diameter of main pulley = 179 mm

Ultimate strength, $S_u = 2220 \text{ Mpa}$

$$\text{Endurance strength, } S_0 = \frac{S_u}{3} = \frac{2220}{3} = 740 \text{ Mpa}$$

Modulus of Elasticity, $E = 207 \text{ Gpa}$

Brinell Hardness, $BHN = 627$

Power available is about 85% of the engine power because the frictional contact between the sides of the belt and the groves result in belt slip.

$$\text{Therefore, Engine Power} = 11.185 \times 0.85 = 9.5 \text{ kW}$$

Pinion and gear are same material; therefore, pinion is weaker. Therefore, base design on pinion.

When two gears mesh, the smaller gear is called the pinion and the larger is the gear. The symbol, D_p will be used for the pitch diameter of the pinion and the symbol, D_g will be used for the pitch diameter of the gear. Then n_p and n_g are used for number of teeth of the pinion and gear respectively.

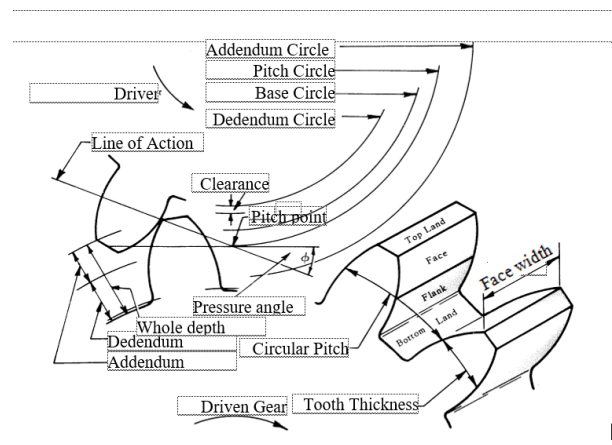


Figure 3. Parts of Gear Teeth

As the gears rotate, the common normal to the surface at the point of contact must always intersect the line of centers at the same point, called the pitch point as shown in Figure 3. The basic requirement of gear tooth geometry is the provision of angular velocity ratios (V.R) that are exactly constant. Manufacturing inaccuracies and tooth deflections will slight deviations in velocity ratio.

$$\text{Pitch circle diameter } D = z \times m = 17 \times 2.5 = 42.5 \text{ mm}$$

$$\text{Outside circle diameter} = (z + 2) \times m = (17 + 2) \times 2.5 = 47.5 \text{ mm}$$

$$\text{Face width (b)} = k_{max} \times \pi \times m = 4 \times \pi \times 2.5 = 31.41 \text{ mm}$$

Diametral pitch = number of teeth / pitch circle diameter
= 17 / 42.5 = 0.4 mm

To find dynamic load, F_d

$$F_t = \frac{M_t}{D_p/2} = \frac{2 \times 74.77}{0.0425} = 3518.59 \text{ N}$$

$$v = \frac{\pi D_p N_p}{60} = \frac{\pi \times 0.0425 \times 1213.4}{60} = 2.7 \text{ m/s}$$

$m = 2.5$, error = 0.01, $C = 119 \text{ kN/m}$ (from Table A.2)

$$F_d = 4398.23 + \frac{21 \times 2.16(24 \times 119 + 4398.23)}{21 \times 2.16 + \sqrt{(24 \times 119) + 4398.23}}$$

$$= 6165.7 \text{ N}$$

To find endurance force, F_0

$$F_0 = S_0 b y_p \pi m$$

$$= 740 \times 10^6 \times 24 \times 10^{-3} \times 0.117 \times 2.5 \times 10^{-3}$$

$$= 16319.94 \text{ N}$$

$$VR = \frac{D_g}{D_p} = \frac{D_g}{42.5} = \frac{n_g}{n_p} = \frac{N_p}{N_g}$$

$$D_g = 2.35 \times 42.5$$

$$= 99.875 \text{ mm}$$

$$N_g = \frac{1213.4}{2.35}$$

$$= 516.34 \text{ rpm}$$

To find ratio factor, Q

$$Q = \frac{2 D_g}{D_g + D_p} = \frac{2 \times 99.87}{99.87 + 42.5} = 1.4029$$

To find wear load, F_w

$$F_w = D_p b K Q$$

$$= 42.5 \times 10^{-3} \times 24 \times 10^{-3} \times 6459.301 \times 10^3 \times 1.4029$$

$$= 9242.98 \text{ N}$$

$$F_d < F_0, F_d < F_w$$

∴ Design is satisfied.

The above calculation is first speed gear design calculation.

3. MODELLING OF SPUR GEAR

Involute spur gears are the most common form of gears which are used to transfer the motion between the parallel shafts. The main concerns while designing an involute spur gear include generation of involute. In earlier days to design an involute spur gear there are many theoretical procedures to draw an approximate involute but no procedure was present to draw a perfect involute for performing analysis. In the present day with the 3-D modeling software's it is easy to generate the involute spur gear with exact involute. The spur gear modeling was done by using SolidWorks software based on spur gear design calculation and modeling diagram shown in Figure 4. In this paper, Carbon Steel is chosen to make the FE model. It has high strength, hardness, good ductility, wear

resistance and moderate ductility. In this study, 40 teeth gear is considered to analyze the Von'mises stress and deflection.

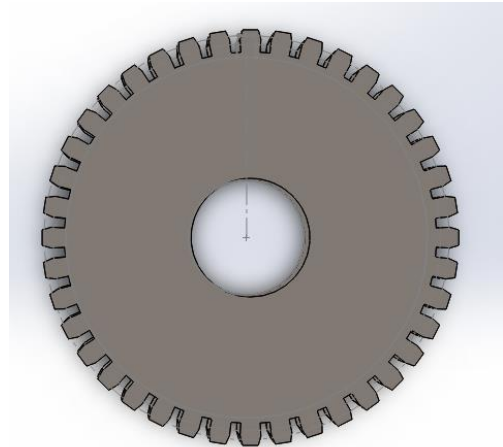


Figure 4. Spur Gear Modeling in SolidWorks

4. Analysis of Gear Tooth

Finite Element analysis for any three-dimensional model is performed in three main steps

1. Pre-processing
2. Solution
3. Post-processing

The pre-processing mainly involves the modeling of the three-dimensional part. The following are the main steps in pre-processing.

1. Engineering Data
2. Geometry
3. Meshing

In an analysis system, the main resource for material properties is engineering data, they can either be experimental or user defined. In this analysis, density and linear elastic properties like Young's Modulus 207 Gpa and Poisson's ratio 0.34 for cast iron are determined. The gear geometry generated from SolidWorks.

For practical considerations the stress on involute spur gear can be better approximated using Finite Element Method [3]. This method can be used in approximating any kind of stress, strains and deformations in single parts and assemblies. Finite element method is a numerical method to obtain approximating solutions to partial differential equations and integral equations. This method originated for solving complex elastic and structural analysis problems.

The first people to develop this method were Alexander Hrennikoff and Richard Courant. In 1947 Olgierd Zienkiewicz coined the term Finite Element Analysis by gathering these methods. In 1952 Boeing made a great effort to analysis the aircraft structures using Finite Element Methods and in 1964 NASA developed a software in Fortran language called Nastran to analysis the aircraft structures. In

mid-1970 due to advancement in computer technology many software's capable of performing Finite element analysis were available.

4.1 Meshing

Meshing is the method of converting continuous models to discrete parts. The goal is to select and locate finite element nodes and element types so that the associated analysis is sufficiently accurate. Element Aspect ratio must be near unity to obtain accurate results.

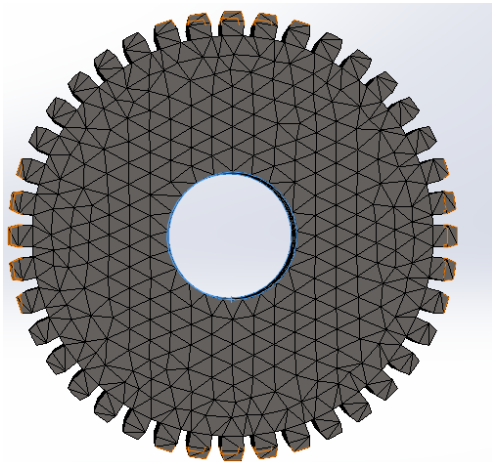


Figure 5. Mesh View of Spur Gear

Tetrahedral elements are used since stress is present all along the thickness of the part. Patch independent algorithm is used since a finer mesh is required around edges and corner. For rest of the body a normal mesh is sufficient and in advanced meshing features the proximity and curvature feature needs to be turned on since the curvature size function examines the curvature on the faces and edges and computes the element sizes so that the element size doesn't exceed the maximum size of curvature angle which are either defined by the user or taken automatically. The minimum size limit is defined as 0.1 in. The proximity size function allows defining the minimum number of element layers in the region that constitute gaps. The stress analysis of spur gear was done by using SolidWorks software, the SolidWorks diagram is shown in Figure 5.

5. RESULTS AND CONCLUSION

Analysis has been carried out by optimizing the material such as carbon steel.

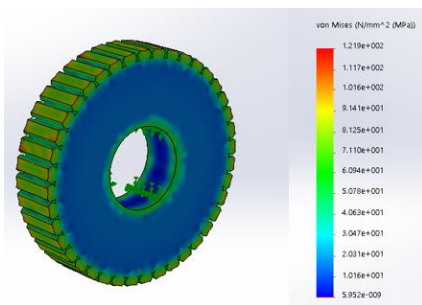


Figure 6. Von'mises Stress of Spur Gear

The results such as total deformation and Von's mises Stress are determined. Comparing the theoretical and numerical has the low values of total deformation, stress and strain. Therefore, it is concluded that carbon steel is suitable for the spur gear manufacturing. The gear is fixed at the center by the fixed support tool. Forces can be applied to the gear by selecting the edge from the graphics window and forces are defined in the component form. The post processing stage involves viewing of data files generated by the software during the solution phase. The Figure 6 displays the stress contour of the gear tooth. Gear tooth may not only break due to bending stress during its life time but develops pits on tooth surface due to high contact stresses fatiguing the surface by compression. Figure 7 and 8 show the deflection and equivalent strain of Spur Gear.

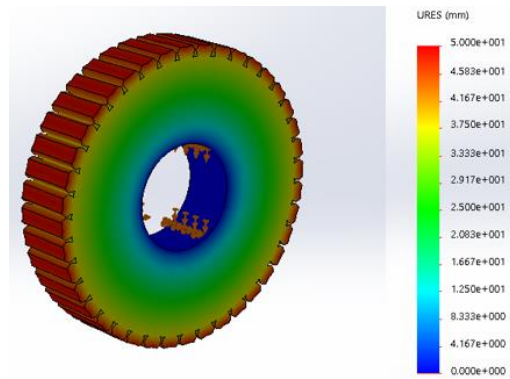


Figure 7. Deflection of Spur Gear

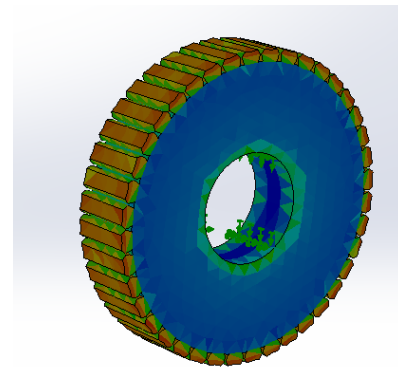


Figure 8. Equivalent Strain of Spur Gear

The maximum stress result obtained from finite element analysis was 122MPa while the maximum deflection obtained from the finite element analysis was 0.05 m under the same conditions. The ultimate stress of steel (C45) is 2220 MPa and the yield stress is 360MPa.

6. ACKNOWLEDGMENTS

The author wishes to express the deepest thanks and gratitude to her respectful teacher Daw Khin Khin Htar, Lecturer of Mechanical Engineering Department of Yangon Technological University. The author special thanks to all who helped her towards the successful completion of this study.

7. REFERENCES

- [1]http://nptel.iitm.ac.in/courses/IIT/MADRAS/Machine_Design_II/pdf/2_1.pdf.
- [2]NASA Reference Publication 1152, AVS COM technical report 84-C-15.
- [3]Design of Machine Elements by C.S Sharma and Kamlesh Purohit
- [4]Finite element Method – its basics and fundamentals by Zienkiewicz, O.C.Taylor, R.L.; Zhu, J.Z.
- [5]Finite Element Analysis by S.S Bhavikatti
- [6]History of Rotating Dynamics by J.S Rao
- [7]Solidwork User’s Guide

Design Trajectory Tracking of Quadrotor using PID controller

Wai Mar Thet
Department of Electronics
Engineering,
Technological University
Thanlyin, Myanmar

Ei Ei Khin
Department of Electronics
Engineering,
Technological University
Thanlyin, Myanmar

Win Thndar Tun
Department of Electronics
Engineering,
Technological University
Thanlyin, Myanmar

Abstract: Autonomous Unmanned Aerial Vehicle (UAVs) have been increasingly employed by researchers, commercial organizations and the military to perform a variety of missions. Drones, also called unmanned aerial vehicles (UAVs), have no human pilot onboard, and instead are either controlled by a person on the ground. With six degrees of freedom (three translational and three rotational) and only four independent inputs (rotor speeds), quadrotors are severely under actuated in order to achieve six degrees of freedom, rotational and translational motion are coupled. This paper examines a conventional PID controller that utilizes a combination of accelerometer and gyro sensors to regulate the orientation of quadrotor UAV and keep the quadrotor auto leveling while flying.

Keywords: UAV, PID controller, quadrotors, accelerometer, gyro sensors.

1. INTRODUCTION

Unmanned Aerial Vehicles (UAVs) are defined as powered aerial vehicles which do not require an on-board pilot to operate but are rather controlled autonomously or remotely. A typical UAV system is comprised of three major components: the aircraft, the ground control station and the operator. Since UAVs can fly without a human pilot on board, they are helpful in missions that do not necessarily need a human's direct oversight. Based on UAVs' capabilities, they were first adopted for military and intelligence missions including deception operations, route and landing reconnaissance, and battle damage assessment. Recently, a large number of UAV applications have also emerged in civil markets. In [4], a camera-equipped mini UAV is used to support wilderness search and rescue. In [5], a large number of swarming UAVs are organized to establish an airborne communication relay. An application of UAV cooperative control is seen in [6], where multiple UAVs are collaborating for map building tasks and in [7] several mini UAVs function as a single unit for surveillance. As a UAV can be autonomously controlled, a powerful controller plays a crucial role in a UAV's development. One of the traditional methods of designing a UAV controller is based on the proportional-integral-derivative (PID) control theory which tunes out an "error" value between a measured state and a desired state of the UAV by adjusting its throttle and control surfaces such as ailerons, elevator, and rudder. Three separate parameters define the PID controller calculation: the proportional value P, the integral value I, and the derivative value D. These values can be interpreted in terms of time: P depends on the present error, I on the accumulation of past errors, and D as a prediction of future errors. This method shows descent performance in short term control by gradually damping the control of the UAV. But a PID controller is only a reactive system which depends on feedback and pre-defined constant parameters and thus it has no direct knowledge of the control process. This paper is organized as follows. Quadrotor UAV modelling that includes aerodynamics concept and configuration are described in Section II includes the conventional PID controller. The experimental testing and result are presented in Section III and conclusion is discussed in Section IV.

2. MODELLING OF A QUADROTOR UAV

2.1 Aerodynamics Forces and Torques

Quadrotor needs a mechanism for generating forces and torques that are required to control its horizontal and vertical movements. There are four main forces that exert on a quadrotor: gravity, lift, thrust and drag. Gravity is a force that pulls the quadrotor down because of its mass. Lift and thrust are the upward reaction forces acting on quadrotor due to the propellers.

Finally, drag is the backward force on the quadrotor due to air. Quadrotor mechanism is mainly based on its rotors and propellers that generate thrust perpendicular to its rotor. The main thrust is generated along Z axis that creates vertical movement. The horizontal movements along X and Y axes are resulted from directing the force or thrust vector in the appropriate direction. Therefore, quadrotor can be characterized by one main control force T and u_F , and three main control torques. The four control inputs are obtained from independently controlling each motor speed. The collective lift u is the sum of the thrust generated by the four propellers.

$$\alpha = \sum_{i=1}^4 f_i \quad (1a)$$

Torque produced by each axis is resulted from

$$\gamma_\theta = b(f_2 - f_4) \quad (1b)$$

$$\gamma_\phi = b(f_3 - f_1) \quad (1c)$$

$$\gamma_\psi = Q_1 + Q_2 + Q_3 + Q_4 \quad (1d)$$

Where b is distance from the propellers to the center of mass of the quadrotor and Q is the fan torques due to air drag.

2.2 Quadrotor Configuration

Quadrotor UAV can be assigned to two different configurations; plus, and cross configuration. In this case, four brushless DC motors are mounted on quadrotor UAV in cross configuration. One pair of motors (1, 3) rotates in counter clockwise direction while the other pair of motors (2, 4) rotates in clockwise direction as shown in fig. The motion of

quadrotor is achieved by varying the motor speed. Thus, increasing or decreasing the four motor's speeds together generates vertical motion. Increasing motor (1, 2) speed or motor (3, 4) speed produces roll rotation that results quadrotor to bend left or bend right. The same method is used for pitch control. Varying motors (1,4) and motors (2,3) speed conversely produce pitch rotation that results quadrotor to go forward or backward. Yaw rotation can be done by the difference in the counter-torque between each pair of motors.

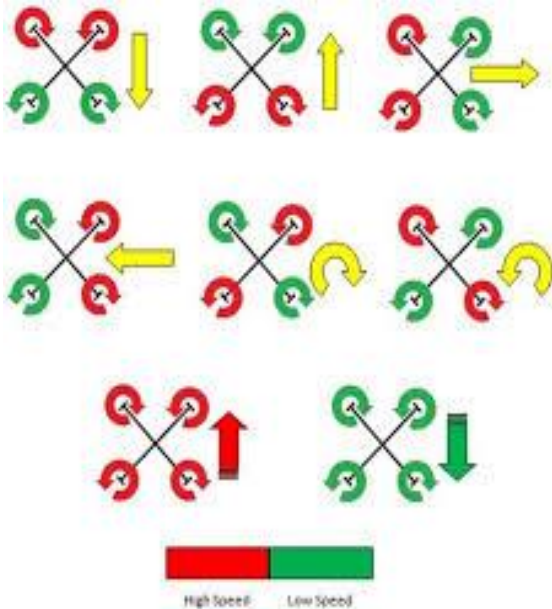


Figure 1. UAV Configuration

2.3 Conventional Pid Controller

The quadrotor in nature is very unstable. In order to stabilize the quadrotor, PID controller is needed to be developed within the system. PID controller is the most widely used controller because of its simplicity and robustness. The mathematical equivalent of PID control algorithm can be expressed as

$$\mu = k_p e + k_i \int edt + k_d \dot{e} \quad (2)$$

Where k_p, k_i , and k_d are the proportional, integral and derivative gains respectively.

To achieve stabilization, three PID controllers are implemented for three different axes: roll, pitch and yaw respectively. For a sensor feedback, we use gyro sensor which is three axes angular rate sensor. $\dot{\theta}^{\circ}_{roll}$, $\dot{\theta}^{\circ}_{pitch}$ and $\dot{\theta}^{\circ}_{yaw}$ are the roll, pitch and yaw angular velocity that can be received from gyro sensor. The error values will be

$$e_{roll} = \theta^{\circ}_{rolldes} - \theta^{\circ}_{roll} \quad (3a)$$

$$e_{pitch} = \theta^{\circ}_{pitchdes} - \theta^{\circ}_{pitch} \quad (3b)$$

$$e_{yaw} = \theta^{\circ}_{yawdes} - \theta^{\circ}_{yaw} \quad (3c)$$

where $\dot{\theta}^{\circ}_{rolldes}$, $\dot{\theta}^{\circ}_{pitchdes}$ and $\dot{\theta}^{\circ}_{yawdes}$ represent desired angular velocity. Using these error values in PID equation, it can be gained

$$\mu_{roll} = k_p e_{roll} + k_d \frac{de_{roll}}{dt} \quad (4a)$$

$$\mu_{pitch} = k_p e_{pitch} + k_d \frac{de_{pitch}}{dt} \quad (4b)$$

$$\mu_{yaw} = k_p e_{yaw} + k_d \frac{de_{yaw}}{dt} \quad (4c)$$

The propeller force on each propeller can be resulted from

$$f_1 \mu_{throttle} + \mu_{pitch} - \mu_{roll} + \mu_{yaw} \quad (5a)$$

$$f_2 = \mu_{throttle} - \mu_{pitch} - \mu_{roll} - \mu_{yaw} \quad (5b)$$

$$f_3 = \mu_{throttle} - \mu_{pitch} + \mu_{roll} + \mu_{yaw} \quad (5c)$$

$$f_4 = \mu_{throttle} + \mu_{pitch} - \mu_{roll} - \mu_{yaw} \quad (5d)$$

where $u_{throttle}$ is the signal pulse received from throttle stick of RC transmitter.

Figure 2 shows the block diagram of quadrotor control system using PID controller. A quadrotor is an under actuated system with four motor for system inputs while it has six degrees-of-freedom which are three translational and three rotational movements. The speed differences of the rotors can generate torques about the roll, pitch, and yaw axes in addition to the thrust that is obtained by the sum of the four rotating propellers.

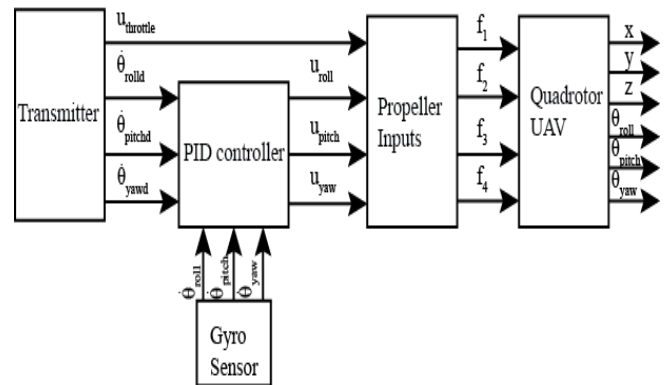


Figure 2. Control scheme of proposed system

3. EXPERIMENTAL RESULTS

For experiment, Arduino Uno which has a clock frequency of 16MHz is used as a microcontroller board. IMU 6050 six DOF sensor is implemented on quadrotor to detect any angle deviation. Four 980 KV brushless DC motor is mounted on each corner for generating thrust that need to lift the quadrotor into the air. For varying the speed of brushless DC motor, electronic speed controller (ESC) is connected to each motor. In order to manage the quadrotor to track the desire position, 2.4GHz 6 channel transmitter is used. The power source for quadrotor is acquired from 3-cell Li-Po battery. All these components are attached firmly to 450mm quadrotor frame and finally the PID controller design is embedded in Arduino controller. The experiment takes place

in indoor area and PC is connected to quadrotor via USB cable to collect data while testing. The experiment has been carried out with three different gain tuning methods. The result plots are illustrated to compare the outcome by employing each method.

Table 1. P gain value

	Roll	Pitch	Yaw
P	5	5	2
I	0	0	0
D	0	0	0

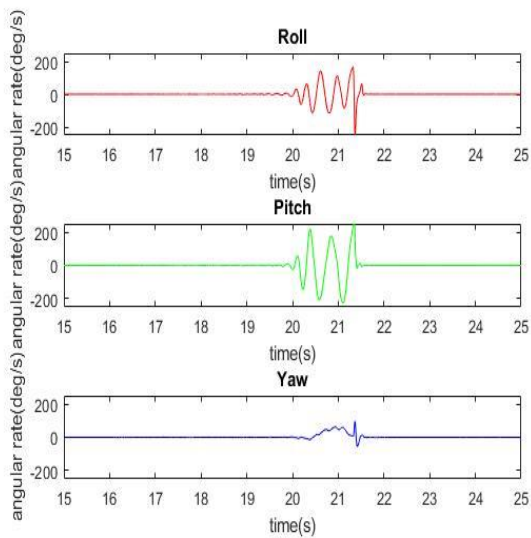


Figure 3. Result of P gain value

1) This result shows the P gain value of time 22s the system is stable for roll, pitch and yaw value. Roll represent for red colour, pitch represent green colour and yaw for blue colour. To start the experiment, the transmitter throttle stick is moved up to let the quadrotor take off vertically and allow the quadrotor to fly about 30 seconds. When the quadrotor reach about one foot above the ground, it becomes vibrate and oscillation occurs. This is because of high proportional gain that creates system overshoot. The angular rate detected by gyro sensor for each axis is represented by individual plot.

Table 2. P gain value

	Roll	Pitch	Yaw
P	1.3	1.3	4

I	0	0	0
D	0	0	0

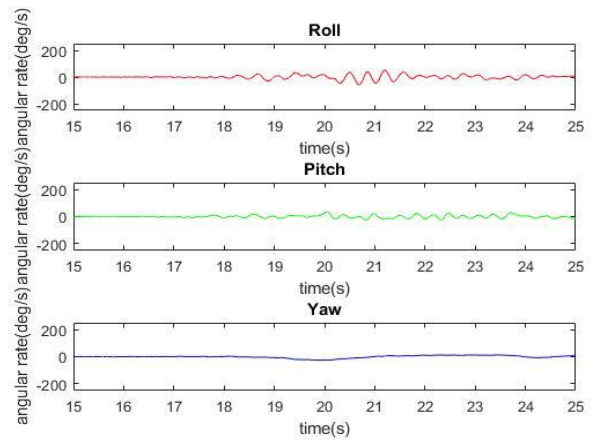


Figure 4. Result of P gain value

2) This result shows the P gain value lower the time of time 24s the system is stable for roll, pitch and yaw value. The data are collected for 10 seconds duration and the experimental plot for manual gain tuning approach. The proportional gain is set to low proportional gain. Error value can be obtained from difference between P gain value for 1.3 and 5 for roll and pitch. Yaw value for 4 and 2. When the absolute error is less than error threshold level, the proportional gain is set to low proportional gain.

Table 3. PI gain value

	Roll	Pitch	Yaw
P	1.3	1.3	4
I	1.5	1.5	5
D	0	0	0

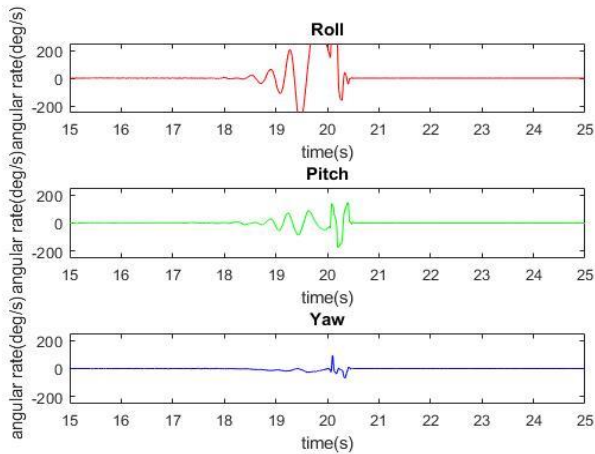


Figure 5. Result of PI gain value

3) This result shows the PI gain value of time 20s the system is stable for roll, pitch and yaw value. proportional gain values for third tuning method.ESC can generate signal pulses from the range of 1000 microsecond to 2000 microsecond.

Table 4. PI gain value

	Roll	Pitch	Yaw
P	1.3	1.3	4
I	1.5	1.5	5
D	0	0	0

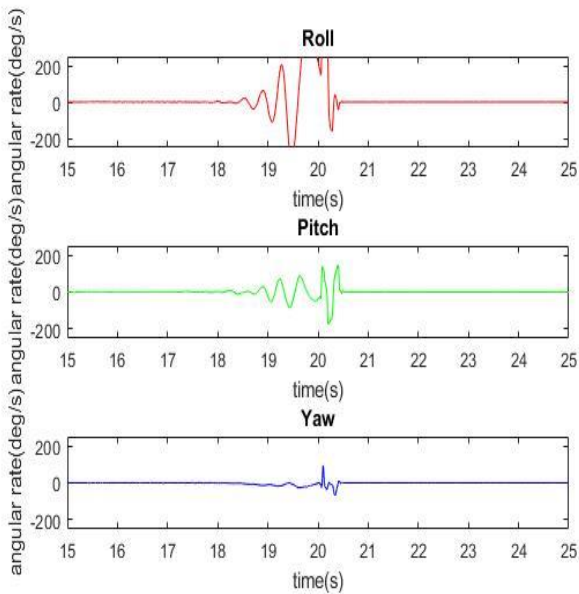


Figure 6. Result of PI gain value

Table 5. PID gain value

	Roll	Pitch	Yaw
P	1.3	1.3	3
I	10	10	5
D	0.08	0.08	0

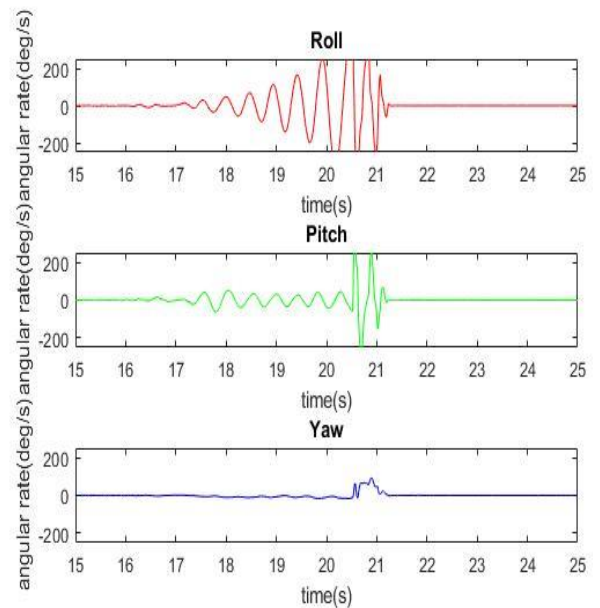


Figure 7. Result of PID gain value

4) This result shows the PID gain value of time 21s the system is stable for roll, pitch and yaw value. proportional gain values for third tuning method.ESC can generate signal pulses from the range of 1000 microsecond to 2000 microsecond. Error value can be obtained from difference between P gain value for 1.3 ,I gain for 10 and D gain for 0.08 for roll and pitch. Yaw for P is 3 and I is 5.

4. CONCLUSION

In this paper three different gain tuning method is used. These are presented to achieve quadrotor stabilization. The experimental tests using three different tuning methods have been carried out to compare the response of quadrotor. Also it can be seen that the quadrotor can manage to stabilize without flipping and crash during indoor testing that has no effect of external disturbances such as wind and other environmental conditions. The next objective is to perform an outdoor flying

test in order to justify which tuning method provides better performance with system enhancement.

5. ACKNOWLEDGMENTS

Firstly, the author would like to acknowledge Dr. Theingi, Rector of Technological University (Thanlyin), for her kind permission to carry out this research work. The authors would like to thank many colleagues from control research group of Department of Electronic Engineering Technological University (Thanlyin). The author particularly wishes to acknowledge all the teachers from Department of Electronic Engineering Technological University (Thanlyin), for their support, encouragement and invaluable guidance in preparation of this research. The authors would like to express their thanks to all preparation period of this paper.

6. REFERENCES

- [1] ApichartSerojanakul and ManopWongsaisuwan, "Optimal Control of Quad-Rotor Helicopter Using State Feedback LPV Method", IEEE, 2012
- [2] S. Bouabdallah and R. Siegwart, "Backstepping and Sliding-mode Techniques Applied to an Indoor Micro Quadrotor", in *IEEE Int. Conf. on Robotics and Automation ICRA '05*, pp. 2259-2264, 2005.
- [3] F. Ruggiero, J. Cacace, H. Sadeghian, and V. Lippiello, "Impedance control of VTOL UAVs with a momentum-based external generalized forces estimator", in *Robotics and Automation (ICRA), 2014 IEEE International Conference*, pp. 2093-2099, 2014.
- [4] Goodrich, A., Morse, S., Gerhardt, D., Cooper, L., Quigley, M., Adams, A. & Humphrey, C. (2008), Supporting Wilderness Search and Rescue using a Camera equipped mini UAV. *Journal of Field Robotics*, 25: 89–110.
- [5] Palat, C., Annamalau, A., & Reed, R. (2005). Cooperative Relaying for Ad-hoc Ground Networks using Swarm UAVs. *Proceedings of IEEE Military Communications Conference 2005*, Vol.3, 1588-1594.
- [6] Yang, Y., Minai, A. (2005). Evidential Map-Building Approaches for Multi-UAV. *Proceedings of American Control Conference 2005*, 116-121.
- [7] Girard, R., Howell, S., & Hedrick, K. (2004). Border Patrol and Surveillance Missions using Multiple Unmanned Air Vehicles. *43rd IEEE Conference on Decision Control*, Vol.1, 620-625.
- [8] A. Tayebi and S. McGillivray, "Attitude stabilization of a four-rotor aerial robots", in *43rd IEEE Conference on Decision and Control*,
- [9] Phillip McKerrow. "Modelling the Draganflyer four-rotor helicopter", in *Proceeding of the 2004 IEEE International Conference on Robotics and Automation*, pp.3596-3601, 2004.

Path Tracking Control of Obstacle Avoiding Robot Using Ultrasonic Sensor

Htike Htike Aung
Department of Mechatronics Engineering
Technological University (Thanlyin)
Thanlyin, Myanmar

Zaw Min Oo
Department of Mechatronics Engineering
Technological University (Thanlyin)
Thanlyin, Myanmar

Abstract: The control algorithm of path tracking is very important for wheeled mobile robot. This paper proposes an algorithm that drives a wheeled mobile robot to a desired path, including obstacle avoidance capabilities. The main objective of this paper is to obtain a collision-free trajectory from the starting point to the target in monitoring environments. In this work, ultrasonic sensors are adopted to implement a real-time obstacle avoidance system for wheeled robots, so that the robot can continually detect surroundings, and avoid obstacles. In this paper, the position of the motor is controlled by using PID controller and PD controller was used in the wall-following method to achieve the optimized path design. In this paper, experimental results of motor control and simulation results for mobile robot's path were shown using MATLAB software. Microcontroller was used as a brain of mobile robot.

Keywords: Wheeled mobile robot, Ultrasonic sensor, Object detection and avoiding, Control algorithm, PID controller, MATLAB simulation, Microcontroller.

1. INTRODUCTION

The sensor-based system is utilized an unknown or changing environment, to perform real-time obstacle avoidance and real-time path planning functions. The sensing elements that are most commonly found in the literature include infrared and ultrasound, CCD camera or CMOS image sensors, laser light pens, global positioning systems (GPS), etc. [1].

Obstacles can be detected by using infrared sensor according to [2], [3]. In Robotino of Festo Didactic, nine infrared sensors are supplied which placed at the both of Robotino 40° apart from each other by Ali, Tariq Younis, and Mohammad M. Ali. The maze solving vehicle is designed with three infrared sensors of which two is used for wall detection to avoid collision and the third is for obstacle detection for picking and placing the objects to clear its pathway with the help of robotic arm by Kamur, Raul, et al. the trajectory path planning on designated path was proposed by Yamada, Taichi, Yeow Li Sa and Akihisa Ohya with the use of laser range scanner, called URG-04LX which has an optimum point distance detection of 4 meters with scanning range of 240 degrees. In these research, in order to get the surrounding environment of robot in all directions, an additional sensor is mounted on the front and back of the robot [4].

Automatically driving for intelligent vehicle requires the integration of many technologies including path planning, position and orientation sensing, path tracking, vehicle control, and obstacle avoidance. Path tracking is the process concerned with how to determine steering and speed settings at each instant of time for the vehicle in order to follow a desired path. Until now, many path tracking algorithms have been proposed for intelligent vehicles or mobile robots [5]. As the robotic vehicle moves along the waypoints from the starting point to the goal point sent from the global motion planner, the local motion planner determines the instant motion of a vehicle. When the local motion planner generates the vehicle's reference motion, difficulties can appear due to the motion constraints of the vehicle. At a low speed of the vehicle, the longitudinal traction and lateral forces which are

exerted on the tires do not exceed the maximum static friction between the tires and the road, preventing the vehicle from moving in the direction orthogonal to its forward direction. Thus the vehicle cannot move directly to the side due to this constraint. Moreover, the minimum turning radius of vehicle exists because of the limited steering angle. These motion constraints make the motion planning problem particularly complex [6]. Thus the local motion planner should generate the feasible local motion for the vehicle without violating the motion constraints. If the constraint equations are written as non-integrable differential expression, then the constraint of this type are known as nonholonomic constraints. The kinematic effect of a nonholonomic constraint is to constrain the direction of the allowable motions at any given point of configuration space. However, the nonholonomic constraint does not reduce the number of dimensions in the configuration space. This means that the vehicle can reach any position and orientation by using the forward and backward motions in the obstacle-free space [6],[8].

Kinematic modeling of the autonomous wheeled mobile robots is analyzed. Then the fuzzy control of a wheeled mobile robot motion in an unknown environment with obstacles is proposed. Output of the fuzzy controller are the angular speed difference between the left and right wheels of the vehicle and the vehicle velocity. Finally, the simulation results show the effectiveness and the validity of the obstacle avoidance behavior in an unknown environment of the proposed fuzzy control strategy by Mester, Gyula [9]. To control the differential drive wheeled mobile robot, PID controller can be used as another way. Agarwal, Kunal, Shadan Mahtab, Sourav Bandyopadhyay, and S. Das Gupta used Proportional-Integral-Derivative (PID) controller to control the navigation of the robots. The most suitable set of values of PID parameters implemented for safe and effective navigation of the robots have been presented. Computer simulation is done using MATLAB software [10].

2. SYSTEM DEVELOPMENT

2.1 Motor Control

The mobility of the obstacle avoiding robot is obtained with two DC geared motors which are attached to the wheels of the car. Control for the two motors in the system is carried out by using the L298N integrated circuit H Bridge. The driving signals are generated by the microcontroller which produces appropriate PWM according to the position of the robot.

2.2 Sensor Placement

Sensor arrangement for object detection, two ultrasonic sensors are used and the arrangement is shown in Figure 1 which is placed at the top and side of the robot. This arrangement is used for accurate detection of object for rectangular shape.

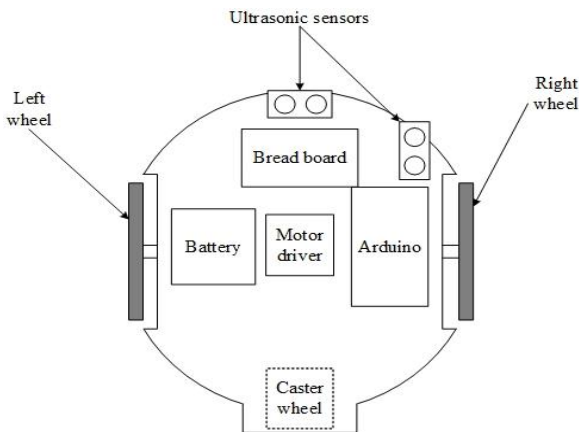


Figure 1. Layout Design of Mobile Robot

In this system, the test robot is a two-wheel mobile robot with differential drive. A caster wheel provides third point contact to ensure stability. The robot is driven by two high speed miniature permanent magnet gear motors coupled to wheels. The robot is battery powered, with the motors supplied with regulated power supply to ensure consistent motor power at all operating scenarios. To move the robot forward, both motors are rotated in the forward direction.

To make the robot turn to the left or to the right, the speed of one motor is reduced. The amount of turn increases as the speed difference increases. Maximum amount of turn is achieved when one motor is turned in a backward direction at maximum speed. This results in maximum speed difference and robot just spin in place. The brain of the robot is an Arduino Mega 2560. Bidirectional motor speed control is achieved by using an H-bridge motor driver circuit. The power applied to the motor is varied by using PWM generated by the microcontroller.

Two ultrasonic sensors are installed on the top of robot and robot's side for object detection. Ultrasonic sensor is used to detect and maintain a specific distance from the object. Ultrasonic sensor generates high frequency sound waves and evaluates the echo which is received back by the sensor. The ultrasonic sensor accurately works with in a range of 4 meters. Ultrasonic sensor operates by calculating the time differences.

Time distance= $\frac{\text{high level time} \times \text{velocity of sound}(340\text{m/s})}{2}$

2

3. ROBOTIC VEHICLE MODEL

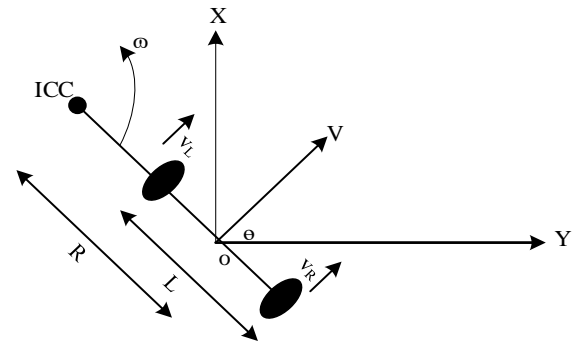


Figure 2 Kinematic Model of Mobile Robot

The kinematics scheme of the differential drive mobile robot is as shown in Figure. 2, where R is the instantaneous curvature radius of the robot trajectory, L is the distance between two driving wheels, ω is the angular velocity of the mobile robot, V is the linear velocity, v_L and v_R are the velocity of the left and right driving wheel, the angle θ indicates the orientation of the robot. For navigation of the robot autonomously it has to know its position at all times, when we change the velocity of the wheels to have different motions the robot must rotate about a point that lies along the common axis of both the driving wheels, this point is known as the Instantaneous Centre of Curvature (ICC). The configuration of the robotic vehicle can be defined as $q = [x \ y \ \theta]^T$. Then the kinematic model of the robotic vehicle is expressed by

$$\dot{q} = \begin{bmatrix} \cos\theta & 0 \\ \sin\theta & 0 \\ 0 & 1 \end{bmatrix} u \quad (1)$$

where $u = [v \ \omega]^T$ is the control input vector that contains the linear velocity and the angular velocity.

In this kinematic model, the motion of the robotic vehicle is constrained by a nonholonomic constraint.

$$x\dot{y} - y\dot{x} = 0 \quad (2)$$

That is, it is assumed that the robotic vehicle is slow enough that the longitudinal traction and lateral force exerted on the tires do not exceed the maximum static friction between the tires and the floor. This is called the no-slip condition [6].

4. PATH TRACKING SYSTEM

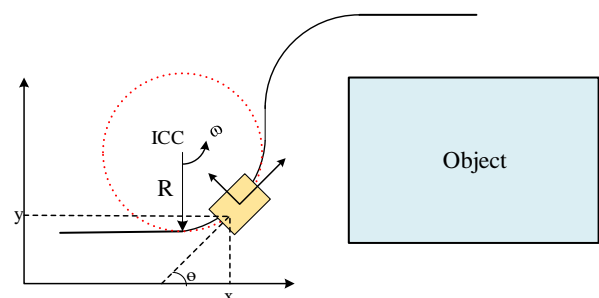


Figure 3. Path Tracking of Mobile Robot

Figure 3 shows the path tracking of mobile robot. The curvature radius of trajectory described by left wheel is $R - \frac{L}{2}$ and right wheel is $R + \frac{L}{2}$. Hence, the following equation hold:

$$\omega(R + L/2) = v_R \quad (3)$$

$$\omega(R - L/2) = v_L$$

Solving for ω and R yields;

$$R = L/2(v_R + v_L)/(v_R - v_L) \quad (4)$$

$$\omega = (v_R - v_L)/L$$

From equation (4) $v(t)$ can be defined as

$$v(t) = \omega(t) \times R = \frac{1}{2}(v_R(t) + v_L(t)) \quad (5)$$

Additionally, dynamic function of the robot are as follows:

$$\begin{aligned} \dot{x}(t) &= v(t)\cos\theta(t) \\ \dot{y}(t) &= v(t)\sin\theta(t) \end{aligned} \quad (6)$$

$$\dot{\theta}(t) = \omega(t)$$

Re-arranged Equation (6) as a matrix yield:

$$\begin{bmatrix} \dot{x}(t) \\ \dot{y}(t) \\ \dot{\theta}(t) \end{bmatrix} = \begin{bmatrix} \cos\theta & \sin\theta & 0 \\ -\sin\theta & \cos\theta & 0 \\ 0 & 0 & 1 \end{bmatrix} \begin{bmatrix} v(t) \\ v(t) \\ \omega(t) \end{bmatrix} \quad (7)$$

where $\dot{x}(t)$ and $\dot{y}(t)$ are transformed point of x, y .

5. PID CONTROLLER DESIGN

PID controller is the mathematically based routine that processes the sensor data and control the position of the robot to keep it on the course. This PID controller is used to control the robot with quick response time and to minimize the overshoot as much as possible [11] and to reduce error between actual and desired position.

A robot without the controller would oscillate a lot about the line, wasting time and battery power. Using the PID controller, the robot will go smoothly keeping its centre always. In straight forward moving, the robot will gradually stabilize itself and this will enable the robot faster and more efficiently. A standard PID controller action can be expressed by

$$u(t) = k_P x e(t) + k_I \int_0^t e(t) dt + k_D \frac{de(t)}{dt} \quad (8)$$

where $e(t)$ = error signal, k_P = proportional gain, k_I =integral gain, k_D =derivative gain. The block diagram of PID controller is described in figure 4.

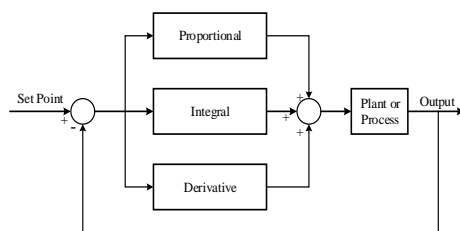


Figure 4. Block Diagram of PID Controller

6. ULTRASOUND OBSTACLE AVOIDANCE STRATEGY DESIGN

When the wheeled mobile robot moves forward along a straight line toward an object, its linear velocity is V and the angular velocity for straight forward motion is $\omega = 0$. After every t sec sampling time, the robot will obtain distance information between the front of wheeled mobile robot and obstacle from ultrasonic sensors $U1$. If $U1$ detects an obstacle straight ahead, and the distance between the two is less than the safe distance (20cm), the robot will stop from moving and start to turn its direction.

If $U1 < 20$,

Then MR stop, MR turn left.

After turning the direction of mobile robot to 90° , the ultrasonic sensor $U2$ is worked. Until object is not missed from $U2$, the mobile robot moves forward and follows by the object. After missing target of $U2$, the mobile robot turns its direction to 90° again. And then, the mobile robot moves straight way and follows by object.

While ($U2=1$)

MR go forward,

While ($U2=0$)

MR turn right.

When the forward direction of the robot is parallel with the obstacles, the wall-following method can be initiated. A PD controller is introduced here to adjust the posture and direction of the front and rear of the robot. The control algorithm of the linear velocity V and the angular velocity ω were designed as follow

If $U2 \geq 20$ cm then MR turn right

$$e_k = d - U2, \quad de_k = e_k - e_{k-1}, \quad \omega_{PI} = k_P e_k + k_{D1} de_k$$

where e_k is the error measurement and e_{k-1} is the previous error measurement of sensor.

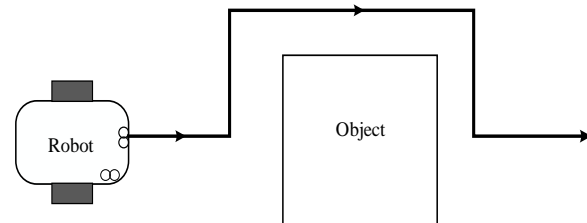


Figure 5. Route of Mobile Robot

The route of the mobile robot is shown in figure 5.

7. EXPERIMENTAL RESULTS FOR POSITION CONTROL

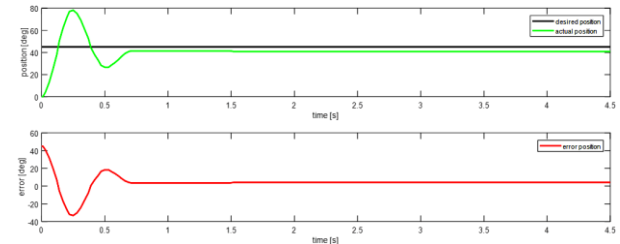


Figure 6. Position Control of DC motor with P Controller

Figure 6 shows only the tuning result of P controller. The proportional response can be adjusted by multiplying the error by a constant K_P . In this figure, the actual result is close to the desired result and there has overshoot and undershoot.

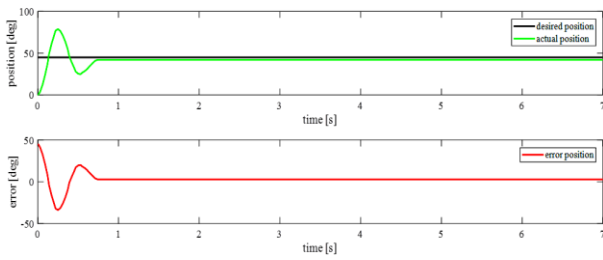


Figure 7. Position Control of DC motor with PI Controller

Figure 7 shows the tuning result of Proportional Plus Integral. In this figure, overshoot and undershoot occurred but the actual result has reached to the desired result. An integral control (K_I) will have the effect of eliminating the steady-state error, but it may make the transient response worse.

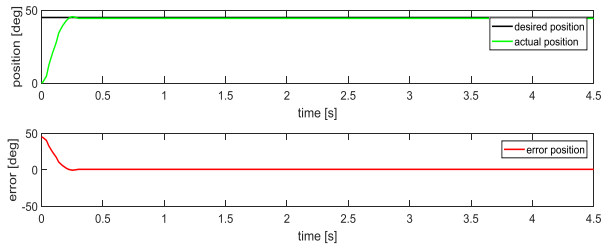


Figure 8. Position Control of DC motor with PD Controller

Figure 8 shows the result of Proportional Plus Derivative. In this figure, the result is almost stable between actual result and desired result. The derivative term slows the rate of change of the controller output. A derivative control (K_D) will have the effect of increasing the stability of the system, reducing the overshoot, and improving the transient response.

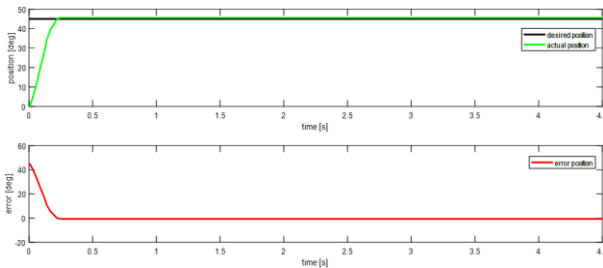


Figure 9. Position Control of DC motor with PID Controller

Figure 9 shows the tuning parameter result of PID controller. By adding PD and PI, the result achieved the good condition. In this result, overshoot disappeared and the actual result reached to the desired condition. The gain of the PID controller can be adjust the reset time for any offset within an acceptable period. Finally, increase the rate of the PID loop until overshoot is minimized. The manual tuning parameter values of DC motor are described in Table 1.

Table 1. Parameter Values for Position Control

Control mode	K_P	K_I	K_D
P	0.114	-----	-----
PI	0.116	0.0000155	-----
PD	0.1185	-----	0.00902
PID	0.1194	0.0000155	0.00905

8. SIMULATION

Figure 10 shows the path tracking of mobile robot plotted in simulation software. In this system, the path of mobile robot is shape in rectangular path because of using the two ultrasonic sensors. In this system, mobile robot moves forward in a straight line and ultrasonic sensor 1 which installed top of the robot senses the object. When object is detected by U1, the robot turns its direction left 90° and U2 sensor measures the distance. After missing the target by U2, the robot turns its direction right 90° and follows by the object. After passing the corner, the robot turns its direction right 90° again, by the use of U2 sensor. And when the robot had spent 5 secs, mobile robot turns its direction to left and go forward. If an object is detected, it will do again.

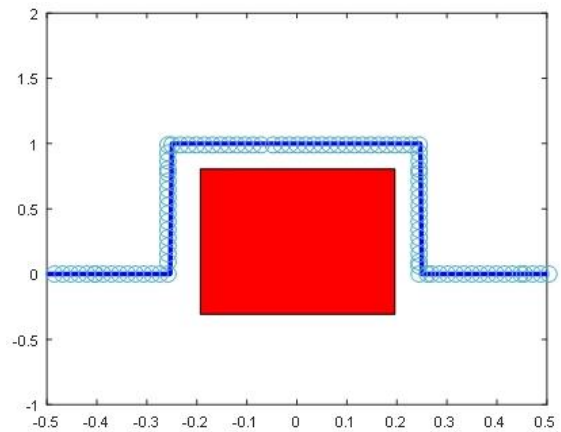


Figure 10. Path Tracking of Mobile Robot

9. CONCLUSION

This paper proposed an algorithm how to track the path of mobile robot using the ultrasonic sensors. The ultrasonic sensor is used to detect and maintain the distance between mobile robot and object. The position control results of obstacle avoiding robot by using PID controller are proposed. The value of PID tuning results are gotten by manually. The manually tuning results are shown using “CoolTerm” software. There has any limitation. This robot used only two ultrasonic sensors, so the mobile robot’s path must be in known environment. As future research, global positioning system (GPS) should also be added to this system how to integrate optical encoders or how to determine the coordinates and orientation of the robot. And then, two ultrasonic sensors are installed in this system. Moreover, by upgrading the sensor integration, the mobile robot can avoid any shape of object and can go to any desired path.

ACKNOWLEDGEMENT

The author is greatly thankful to Dr.Theingi, Rector of Technological University Thanlyin, for her encouragement, invaluable permission and her kind support in carrying out this paper work. The author is deeply grateful to all the teachers from Department of Mechatronic Engineering, Technological University(Thanlyin), who work in Research. For their support, encouragement and all persons who have given support during the preparation period of this research work.

REFERENCES

- [1] T. F. Wu, P. S. Tsai, N. T. Hu, and J. Y. Chen. "Use of ultrasonic sensors to enable wheeled mobile robots to avoid obstacles." In *Intelligent Information Hiding and Multimedia Signal Processing (IIH-MSP), 2014 Tenth International Conference on*, pp. 958-961. IEEE, 2014.
- [2] T. Y. Ali, and M.M. Ali." Robotino Obstacles Avoidance Capability Using Infrared Sensors." in *Applied Electrical Engineering and Computing Technologies(AEECT), IEEE Jordan Conference*, pp. 1-6. 2015.
- [3] R. Kumar, P. Jitoko, S. Kumar, K. Pillay, P. Prakash, A. Sagar, R. Singh, U. M., Raul." Maze solving robot with automated obstacle avoidance." *Procedia Computer Science* 105,pp. 57-61.2017.
- [4] T. Yamada, Y.L. Sa, and A. Ohya." Moving obstacle avoidance for mobile robot moving on designated path." in *Ubiquitous Robots and Ambient Intelligence (URAI),2013. 10th international conference on* pp. 509-514. IEEE 2013.
- [5] J. Duan, J. Yao, D. Liu, and G. Liu. "A path tracking control algorithm with speed adjustment for intelligent vehicle." In *Robotics and Biomimetics (ROBIO), 2013 IEEE International Conference on*, pp. 2397-2402. IEEE, 2013.
- [6] D.-H. Kim, C.-S. Han, and J. Y. Lee. "Sensor-based motion planning for path tracking and obstacle avoidance of robotic vehicles with nonholonomic constraints." *Proceedings of the Institution of Mechanical Engineers, Part C: Journal of Mechanical Engineering Science* 227, no. 1 (2013): 178-191.
- [7] S. K. Malu, and J. Majumdar. "Kinematics, localization and control of differential drive mobile robot." *Global Journal of Research in Engineering* (2014).
- [8] M. Cui, D. Sun, W. Liu, M. Zhao, and X. Liao. "Adaptive tracking and obstacle avoidance control for mobile robots with unknown sliding." *International Journal of Advanced Robotic Systems* 9, no. 5 (2012): 171.
- [9] G. Mester." Obstacle voidance of mobile robot in unknown environment." in *Intelligent System and Inormatics (SISY) 2007.5th International Symposium on* pp.123-127. IEEE.
- [10] K. Agarwal, S. Mahtab, S. Bandyopadhyay, and S. D. Gupta." A proportional-integral-derivative control scheme of mobile robotic platform using Matlab." *IOSR Journal of Electrical and Electronics Engineering* .7. pp.235-240.2013.
- [11] M. Rokonzaman, S. M. Ferdous, E. G. Ovy, and Md. Hoque. "Smooth Track-Keeping and Real Time Obstacle Detection Algorithm and its PID Controller Implementation for an Automated Wheeled Line Following Robot." In *Advanced Materials Research*, vol. 201, pp. 1966-1971. Trans Tech Publications, 2011.